Implementation of the EPICS2017 database for photons in Geant4

Zhuxin Li, Claire Michelet, Sebastien Incerti, Vladimir Ivanchenko, Mihaly Novak, Susanna Guatelli, Hervé Seznec

Implementation of the EPICS2017 database for photons in Geant4

Zhuxin Li[a], Claire Michelet[a], Sébastien Incerti[a], Vladimir Ivanchenko[b, c], Mihaly Novak[c], Susanna Guatelli[d], Hervé Seznec[a]

[a] CNRS, Université Bordeaux, CENBG, UMR5797, F-33170 Gradignan, France

[b] Tomsk State University, 634050 Tomsk, Russia

[c] CERN, CH1211 Geneve 23, Switzerland

[d] Center for Medical and Radiation Physics, University of Wollongong, New South Wales, 2522, Australia

Emails:

Zhuxin Li: li@cenbg.in2p3.fr

Claire Michelet: michelet@cenbg.in2p3.fr

Sébastien Incerti: incerti@cenbg.in2p3.fr

Vladimir Ivanchenko: Vladimir.Ivantchenko@cern.ch

Mihaly Novak: mihaly.novak@cern.ch

Susanna Guatelli: susanna@uow.edu.au

Hervé Seznec: seznech@cenbg.in2p3.fr

Corresponding author:

Zhuxin Li (li@cenbg.in2p3.fr)

Abstract:

This paper describes in detail the implementation of Geant4 Livermore electromagnetic physics models based on the EPICS2017 database for the low energy transport of photons. These models describe four photon processes: gamma conversion, Compton scattering, photoelectric effect and Rayleigh scattering. New parameterizations based on EPICS2017 were performed for scattering functions of Compton effect, subshell cross-sections of the photoelectric effect and form factors of Rayleigh scattering, in order to improve the precision of fitted values compared to tabulated values. Comparisons between new and old parameterizations were also carried out to evaluate the precision of the new parameterizations. The models were tested through a comparative study, in which the mass attenuation coefficient was calculated for both total photon interaction and each process using Geant4 simulations based on EPICS2017 and EPDL97 respectively. The results obtained from the simulations were found in good agreement with the XCOM reference data.

Keywords: Geant4, EPICS2017, Livermore, XCOM, mass attenuation coefficient

1. Introduction

Geant4 is an open-source Monte Carlo toolkit for the simulation of particle interactions with matter [1-3]. Originally designed to answer the needs of high energy physics, including the CERN experiments ATLAS and CMS (which discovered the Higgs boson in 2012), Geant4 has been found useful in other fields, such as space exploration and medical physics. The development of parallel computing has given

a way to improve execution speed efficiently, leading to an expansion of the capabilities to the description of more and more complex phenomena. Geant4 provides a low energy electromagnetic sub-package dedicated to improve the accuracy and precision of simulations at low energies below 1 GeV [4, 5]. It includes complementary and alternative physics models according to the energy range, describing the electromagnetic interactions of photons (gamma conversion, Compton scattering, photoelectric effect and elastic scattering), electrons and positrons (ionization and Bremsstrahlung) as well as annihilation for positrons. Two main sets of models are available in this sub-package: *i)* Penelope [6] implemented in C++; *ii)* Livermore.

Livermore physics models constitute an important component of the sub-package and are based on three evaluated data libraries of the Lawrence Livermore National Laboratory (LLNL) for elements with atomic number Z = 1-100: *i)* EPDL97 (Evaluated Photons Data Library) [7], *ii)* EEDL (Evaluated Electrons Data Library) [8], *iii)* EADL (Evaluated Atomic Data Library) [9]. These models have been utilized in space radiation [10], archeology [11] and medical physics applications, particularly in radiotherapy [12, 13], micro-and nanodosimetry [14, 15], imaging [16, 17] and spectrometry [18, 19]. Especially for medical physics, it is now possible to model the interaction of particles with living matter down to the molecular level (DNA), opening the way to a finer understanding of the mechanisms occurring during and following irradiation [20]. For these reasons, the use of Geant4 in this field is now quickly growing, especially in the frame of the optimization of novel techniques of radiation therapy (for instance for image guided radiotherapy and for proton/hadron-therapy). Livermore models are also adopted in the Geant4-DNA set of physics models [21-24] and by other medical physics oriented simulation platforms based on Geant4, like TOPAS (*http://www.topasmc.org*) [25, 26], GATE (*http://www.opengatecollaboration.org*) [27, 28] and GAMOS (*http://fismed.ciemat.es/GAMOS/*[29, 30]. Comprehensive validations have been performed by the Geant4 community for photon cross-sections [31, 32] and more specifically for medical applications [33]. These benchmarking tests compared Livermore models with respect to different well-known databases, such as XCOM [34], SANDIA [35], Penelope [6], in the 1 keV - 100 GeV energy range. This range corresponds to the data available in the XCOM library. Poon *et al*. [36] carried out a validation specifically for water and tungsten in the 1 keV - 100 MeV energy range for radiotherapy physics applications. Furthermore, some studies compared simulated results based on Livermore models with XCOM data and experimental data for specific energy values, using radioactive sources in the keV - MeV energy range, for typical biological, geological and industrial materials [37-39]. All these publications have highlighted the applicability of the Livermore models.

However, the EPDL97, EEDL and EADL libraries, which were designed in the 1990's, have undergone a major updating process resulting in a new version, EPICS2017 (Electron-Photon Interaction Cross Sections) (*https://www-nds.iaea.org/epics/*) [40]. It is important that Geant4 takes into account these new databases to improve the precision and reliability of models. An important change in EPICS2017 is the interpolation of tabulated data. Linear interpolation is adopted to calculate physical quantities between tabulated values in EPICS2017 instead of logarithmic interpolation. Thus, there is generally an increase in the number of tabulated points. In Geant4, the data are either directly used as tabulated values, after a conversion to a specific Geant4 format, or parametrized to improve speed and memory management, especially when the data vary smoothly. The increase in the number of points in EPICS2017 allows the existing parameterizations to be improved. Another main modification in EPICS2017 concerns the cross-sections for the photoelectric effect and Rayleigh scattering, resulting from a major change in the atomic binding energies. It is thus important that Geant4 can benefit of this major update.

This paper describes in detail the implementation of EPICS2017 database for four photon processes: gamma conversion, Compton scattering, photoelectric effect and Rayleigh scattering. The database is used for the determination of cross-sections and sampling of the final state. The updated physical quantities include: total cross-sections for all the processes, subshell cross-sections for the photoelectric effect, scattering functions for Compton scattering and form factors for Rayleigh scattering. Regarding the cross-section data, it should be noted that in spite of the wide energy range of the cross-sections, extending from 1 eV to 100 GeV, it is strongly recommended not to use EPICS2017 below 100 eV due to the degradation of the accuracy of the database [41] . Besides, data uncertainty must be addressed when it comes to a database. It is stated that it is rather difficult to estimate the uncertainty in a realistic way since the database is based on theoretical and experimental data. However, an indication of uncertainty can be estimated by comparing EPICS2017 with several well-known and widely-used databases, such as XCOM [41]. The estimated uncertainties are specified in the following sections relevant to each process. After the implementation, a comparative study using Geant4 simulations was performed. The mass attenuation coefficient was calculated for both total photon interaction and each process using Geant4 10.6 implementing EPDL97 and the Geant4 11.0 release implementing EPICS2017. The reason why we used Geant4 10.6 instead of 10.7 is that the gamma conversion process has been already updated with EPICS2017 in Geant4 10.7, while other processes have not. It is worth noting that a flag of Livermore data is created in the list of EM parameters in the Geant4 11.0 release so that users can still use EPDL97 database if they wish, by using the UI command "***/process/em/LivermoreData argument***" in the input macro. This command line refers to EPDL97 database if ***argument*** is "**livermore**", or EPICS2017 database if ***argument*** is "**epics_2017**". The principal aim of the present study is, on one hand, to assess quantitatively the compatibility of Geant4 Livermore models in Geant4 11.0 versus 10.6; on the other hand, to demonstrate the accuracy and reliability of the cross-section data with respect to the reference XCOM data.

2. Implementation for each process

2.1. Gamma conversion

2.1.1. Physical process

Gamma conversion occurs when a photon interacts with a strong electric field from either a nucleus (pair production) or an electron (triplet production) of the atom. Gamma conversion can possibly occur only above a photon energy threshold of 1.022 MeV for pair production, and above 2.044 MeV for triplet production. At high photon energies, above 10 - 100 MeV, depending on the Z of material, it becomes the dominant process. At very high energies, pair and triplet production show very simple atomic number (Z) dependence: pair production varies as Z^2, and triplet production as Z. For this reason, triplet production is more important for low Z elements. For example, for hydrogen (Z = 1), the cross-sections of pair and triplet production are almost equal, while for lead (Z = 82), pair production is roughly 82 times larger than triplet production. In Geant4, the total cross-section of gamma conversion is the sum of pair and triplet production.

2.1.2. Description of the data

EPICS2017 contains tabulated cross-section data for pair and triplet production. The only difference compared with EPDL97 is that more points are contained in EPICS2017 in order to allow the use of linear interpolation between tabulated points. We performed a comparison of cross-sections for pair and triplet production for all the elements between EPICS2017 and EPDL97, while three materials (H, Al, Pb) were arbitrarily chosen only for illustration (Fig. B1 in Appendix B). The cross-sections of

EPICS2017 were shown in a close agreement with those available in Penelope and with XCOM data for all elements (Z = 1 to 100), within a maximal relative difference smaller than 1% [41].

2.1.3. Implementation

For the gamma conversion process, we updated two model classes in the Livermore low-energy sub-package: ***G4LivermoreGammaConversionModel*** and ***G4LivermoreGammaConversion5DModel.*** They both perform the following tasks: *i)* calculate the cross-section according to the energy value of the incident gamma and the composition of material; *ii)* generate the final state (*e.g*. energy and direction of primary and secondary particles).

The calculation of the cross-section for both classes is based on the tabulation of EPICS2017 data using linear interpolation. As mentioned before, the tabulated cross-section data encompass pair production and triplet production. Since the tabulated energy values are different between pair and triplet production, a linear interpolation was carried out on triplet cross-section data to acquire the data points corresponding to the tabulated pair production data, and calculate the sum of cross-sections. The difference between the two models lies in the way of sampling the final state: *i)* ***G4LivermoreGammaConversionModel*** is derived from ***G4PairProductionRelModel***, and thus inherits its method of sampling the final state, in which the Landau-Pomeranchuk-Migdal effect is taken into account; *ii)* ***G4LivermoreGammaConversion5DModel*** is a new model class, inheriting a more complex description of the final state, provided by ***G4BetheHeitler5DModel***. More precisely, ***G4BetheHeitler5DModel*** takes into account the recoil target (isolated-charge or atomic) for nuclear or triplet conversion, and also the polarization of the incident photon if required [42]. For this reason, it is more accurate but slower than other alternative models. Users should choose the appropriate model according to their needs.

2.2. Compton scattering

2.2.1. Physical process

The Compton scattering is an inelastic gamma scattering on an atom with the ejection of an electron. It is a prominent process in the MeV range, particularly for low Z elements. A scattering function is used to describe the angular distribution of the incoherently scattered photon [43, 44]. It is defined as a function of momentum transfer q, which is expressed as:

$$q = \frac{1}{\lambda} sin(\frac{\theta}{2}) \qquad (1)$$

where θ is the photon scattering angle and λ is its wavelength.

At low momentum transfers, the scattering function approaches zero and at high momentum transfers it approaches a constant value, the atomic number Z of the element.

2.2.2. Description of the data

EPICS2017 contains tabulated cross-section data and scattering function data. For cross-section and scattering function, the only difference with EPDL97 is that more points are contained in EPICS2017 in order to allow one to use linear interpolation between tabulated points. In addition, we should note that the momentum transfer in the scattering function is expressed in the unit cm^{-1} in EPDL97, while 10^{16} m^{-1} in EPICS2017. Three materials (H, Al, Pb) for comparisons of cross-sections and scattering functions between EPICS2017 and EPDL97 are shown in the Fig. B2. A good agreement was observed when comparing EPICS2017 with Penelope and XCOM data for all elements (Z = 1 to 100). Roughly, a 4% difference for cross-sections was observed in the 100 keV to 1 GeV range. At lower energies, it was shown that EPICS2017 and XCOM data remain in a very good agreement down to 1 keV, whereas the

difference with Penelope data increases. However, in this low energy range, the process of incoherent scattering represents less than 1% of total absorption for low Z elements, even much less for high Z elements [41].

2.2.3. Implementation

Compton scattering is described by ***G4LivermoreComptonModel*** below 1 GeV. Above 1 GeV, the Klein-Nishina model is used instead, by ***G4KleinNishinaModel***. Cross-section data are tabulated and read by ***G4LivermoreComptonModel***. Scattering functions, *SF*, however are not tabulated but parameterized on several regions depending on the values of momentum transfer, *q* (Fig. 1). The scattering functions are parametrized in the following way:

- For regions 1 and 2, a polynomial fit is used:

$$log_{10} SF = \sum_{i=0}^{n} a_i \, (log_{10} \, q)^i \qquad (2)$$

Where n is the degree of polynomial, a_i is the fitting parameter.

- For region 3:

$$SF = Z \qquad (3)$$

Where Z is the atomic number of the element.

Our aim was to improve the accuracy of these parameterizations; this was achieved in two steps: *i)* modification of the regions; *ii)* modification of the degree of the polynomial functions when necessary. In Geant4 10.6, n = 1 for region 1, n = 3 for region 2. In our implementation, the region 2 was divided into 2 parts with n = 4 for each sub-region (Fig. 1). The limits of different regions were taken from Geant4 10.6 and adjusted accordingly. A special attention was paid to avoid discontinuity of relative difference values at the junction of two consecutive regions.

Three materials (H, Al, Pb) for comparisons of fits are given in Fig. B3. The relative difference in percentage of fitted values compared to tabulated data is calculated as follows:

$$\text{Relative difference } (\%) = \frac{\text{Fitted value} - \text{Tabulated value}}{\text{Tabulated value}} \times 100 \qquad (4)$$

The maximal relative difference between parametrized and tabulated SF as a function of Z is shown in Fig. 2. We observed that the maximal relative difference amongst all elements is about 0.0053% (Z = 32) in region 1 and 6.5% (Z = 38) in region 2 for Geant4 11.0, compared to approximately -20% (Z = 2) and -42% (Z = 91) for Geant4 10.6. However, due to the presence of outliers, it would be misleading if we directly compare these maximal values. For this reason, we tried to estimate an indicative value of the improvement of precision of fit (*IP*) on average for both region 1 and region 2. The *IP* is calculated as follows:

$$IP = \frac{1}{100} \sum_{i=1}^{100} \left| \frac{(R_{max})_i}{(r_{max})_i} \right| \qquad (5)$$

Where *i* is the atomic number of elements, varying from 1 to 100, $(R_{max})_i$ and $(r_{max})_i$ are the maximal relative difference in percentage of the *i*-th element for Geant4 10.6 and 11.0 respectively. The relative difference is expressed as equation (4).

Eventually, we found an *IP* about 1000 for region 1 and 2.8 for region 2. We have to point out that an IP of 1000 for region 1 does not mean that the previous fitting method was bad: in fact, the relative difference using previous fitting method was acceptable for two reasons: i) the maximal relative differences of fitted values compared to tabulated values were not too big, about 5-10% for most elements as shown in Fig. 2; ii) the values of scattering function in region 1, which is a low q momentum transfer region, are much smaller as shown in Fig. B2 in Appendix B, so the consequence on Geant4 simulation results would be negligible compared to the other fitting regions.

2.3. Photoelectric effect

2.3.1. Physical process

The photoelectric effect is the ejection of an electron from an atom after a photon has been absorbed. It is the dominant process at low energy, up to a few hundred keV, for most elements. The electron kinetic energy is the difference between the incident photon energy and the binding energy of the electron. In order to model the ionized subshell, from which the electron is emitted, the cross-sections of each subshell are required in addition to total cross-sections.

2.3.2. Description of the data

One of the main modifications in EPICS2017 concerns the cross-sections, both total and subshells, for the photoelectric effect. This modification results from a major change in EPICS2017 regarding the atomic binding energies. These new binding energies result in the shift of the photoelectric edges and consequently leads to a modification of the photoelectric cross-sections. Three materials (H, Al, Pb) for comparisons of binding energies and total cross-sections between EPICS2017 and EPDL97 are shown in Fig. B4 and Fig. B5 respectively. The relative difference in percentage for binding energies and total cross-sections is calculated as follows:

$$\text{Relative difference (\%)} = \frac{\text{EPICS2017} - \text{EPDL97}}{\text{EPDL97}} \times 100 \quad (6)$$

It should be noticed [41] that the cross-section values were modified only within the edge regions, in order to keep the good agreement that had been already observed for EPDL97 with experimental data. The shifts are largest for high Z elements. It was concluded that EPICS2017 is in agreement with the XCOM and SCOFIELD data sets. However, when comparing to Penelope, a larger difference is observed at high energy, above a few hundred keV; the difference even reaches 15 % for some elements, whereas it is 1-2% when compared XCOM and SCOFIELD [41].

We observed large relative differences in binding energies for outer subshells (Fig. B4). However, these large differences do not have great impact, since the binding energies of the outer subshells are small, within a few eV. Considering the cross-sections, they were modified near the photoelectric edges, in order to adjust to these modifications of binding energies. The maximal relative difference of binding energies was plotted as a function of Z for all elements (Fig. 3). Large variations were observed, up to 71%, for Z = 71, due the large differences observed for the outer subshells. In order to compare the data in a more representative way, we also plotted the mean absolute relative difference (*MD*) as a function of Z (Fig. 3), calculated as follows:

$$MD = \frac{1}{n}\sum_{i=0}^{n-1} |r_i| \quad (7)$$

Where n is the number of subshells of an element, r_i is the relative difference of binding energy of the *i*-th subshell. The relative difference is expressed as equation (6).

We would like to point out that the binding energies for outer subshells are more prone to variations, depending on the molecular state of the material. The purpose of EPICS2017 and EPDL97 is to provide atomic data for engineering applications, keeping in mind that the elements are considered as cold, neutral, isolated atoms. In Geant4, in most cases, molecular cross-sections are derived from a linear combination of atomic cross-sections according to the atomic fractions. So, it would be interesting in the future to provide experimental data in Geant4 for molecular materials. Note that water is already treated as a molecule in the Geant4-DNA extension of Geant4 [21].

2.3.3. Implementation

The photoelectric effect is described by ***G4LivermorePhotoElectricModel***. The total and subshell cross-sections are either described by a parameterization or directly tabulated, depending on the energy of the incident photon *E*. More precisely, the cross-sections are tabulated when energy is lower than a threshold (low energy limit E_a in Fig. 4). Above the threshold (low energy limit), cross-sections are parametrized. The thresholds and energy intervals are adjusted based on those defined in Geant4 10.6, according to the element. Parameterizations are performed on the subshell cross-sections in two different energy intervals ("low energy fit" and "high energy fit") (Fig. 4), as follows:

$$\sigma_i(E) = \sum_{j=1}^{6} \frac{a_{ij}}{E^j} \qquad (8)$$

Where a_{ij} is the fitting parameter corresponding to the *i*-th subshell and the *j*-th degree of polynomial; *E* is the energy of photon.

Thus, the total cross-sections are obtained by the following equation:

$$\sigma_{tot}(E) = \sum_{i=0}^{n-1} \sigma_i(E) = \sum_{i=0}^{n-1} \sum_{j=1}^{6} \frac{a_{ij}}{E^j} \qquad (9)$$

Where *n* is the number of subshells.

Three examples (H, Al, Pb) of fitted ***K shell*** cross-sections using new fitting parameters, compared with tabulated values, are given in Fig. B6. The relative difference in percentage is calculated in the same way following equation (4). In order to evaluate the performance of our new fits, we plotted the maximal relative difference amongst all the subshells, as a function of Z, in Fig. B7. The values are of the same order of magnitude for the "low energy fit" and are slightly improved for the "high energy fit". The highest values in the present work are up to -6.7% for the element Z = 59, compared to -7.6% for the element Z = 59 for Geant4 10.6. These high values especially occur for the outer subshells. For this reason, in order to show the quality of the fits from an overall perspective, we calculated the mean absolute relative difference value (MD) as a function of Z (Fig. B8), according to the following formula:

$$MD = \frac{1}{nm} \sum_{i=0}^{n-1} \sum_{j=1}^{m} |r_{ij}| \qquad (10)$$

Where *n* is the number of subshells, *m* is the number of energy points, r_{ij} is the relative difference at the *j*-th energy point of *i*-th subshell. The relative difference is expressed as equation (4).

The highest values in the present work for subshell cross-sections are up to 0.96% for the element Z = 12, compared to 0.98% for the element Z = 3. From a technical point of view, it is difficult to make both fits without having to make a compromise. Especially, particular attention was paid to avoid cross-section jumps at the border between the low and high energy fits.

Finally, for total cross-sections, the maximal relative difference as a function of Z is displayed in Fig. 5. The highest values in the present work are up to 4.2% for the element Z = 10, compared to 4.4% for Geant4 10.6 for the element Z = 93. Based on these maximal relative differences, we tried to estimate an indicative value of the improvement of precision of fit (IP) on average for both low and high energy fits, following equation (5). We obtained an IP of about 1.9 for the low energy fit and 1.3 for the high energy fit.

2.4. Rayleigh scattering

2.4.1. Physical process

Rayleigh scattering is an elastic scattering of a photon off atomic electrons without change in its wavelength. In general, this process plays a significant role in the low energy range. The change in photon direction is described for each element using a form factor that gives the angular distribution of the scattered photon [44, 45]. The form factor is a function of the momentum transfer, q, which, as for Compton scattering, is defined in the same way as equation (1). At high momentum transfers, the form factor approaches zero and at low momentum transfers it approaches a constant value, the atomic number Z of the element.

2.4.2. Description of the data

Coherent cross-sections constitute another major change in EPICS2017. This is also due to the modification of binding energies already mentioned for the photoelectric effect. However, modifications for the cross-sections of the photoelectric effect were restricted to the vicinity of edges, whereas a complete update has been performed for the cross-sections of Rayleigh scattering. For this reason, it should be noted that, unlike the data for other processes, the number of tabulated points for Rayleigh scattering cross-sections in EPICS2017 is lower than that in EPDL97. Batic *et al.* [46] compared available experimental Rayleigh scattering cross-sections with EPDL97 for several elements; obvious discrepancies were observed, especially for Z = 18. Similarly, we compared EPICS2017 with some of the experimental data based on [46] for Z = 18, which showed that EPICS2017 values are much closer to experimental measurements than EPDL97. It would be out of the scope of this work to make a review of the existing experimental data. However it would be interesting in future studies to make a more systematic and precise comparison. Considering form factors, the only difference between EPICS2017 and EPDL97 occurs in the increase of tabulated points. Three examples (H, Al, Pb) of comparisons of cross-sections and form factors for Rayleigh scattering between EPICS2017 and EPDL97 are shown in Fig. B9.

2.4.3. Implementation

Rayleigh scattering is described by ***G4LivermoreRayleighModel***. It is used to generate the final state of the scattered photon after interaction using form factors (FF), which are parametrized as a function of the momentum transfer q, as follows [44]:

$$FF^2(q) = \sum_{i=0}^{2} \frac{a_i}{(1 + b_i q^2)^{N_i}} \quad (11)$$

Where a_i, b_i, N_i are fitting parameters.

New fitting parameters were recalculated based on EPICS2017 with respect to the same function, to take into account the increase of data points. The fit is performed at low q only when the FF is high enough, more precisely: $FF^2 \geqslant 10^{-6} \cdot Z^2$, where Z is the atomic number. Moreover, as FF quickly decreases down to zero at high momentum values, the precision of fit was optimized so that the relative difference between fitted and tabulated data is smaller in the low q region (high FF values)

than in the high *q* region. The relative difference in percentage between fitted and tabulated FF^2 is calculated as follows:

$$\text{Relative difference (\%)} = \frac{\text{Fitted FF}^2 - \text{Tabulated FF}^2}{\text{Tabulated FF}^2} \times 100 \quad (12)$$

Three examples (H, Al, Pb) of comparisons of relative difference of fits are given in Fig. B10. It is conspicuous in these examples that the maximal relative difference between fitted and tabulated FF^2 values varies depending on *q*: as already explained, the relative difference is much larger at high *q*, which actually has little impact because it corresponds to low FF values. For this reason, the maximal difference obtained for each element is not representative. Thus, we calculated the mean absolute relative difference value (*MD*) for each element (Fig. 6):

$$MD = \frac{1}{m}\sum_{j=1}^{m}|r_j| \quad (13)$$

Where *m* is the number of fitted points, r_j is the relative difference at the *j*-th point. The relative difference is expressed as equation (12).

We observed a slight improvement in the accuracy of parameterization. The maximal value is about 16% (Z = 48) for Geant4 11.0, whereas 35% (Z = 18) for Geant4 10.6. We also tried to estimate an indicative value of the improvement of precision of fit (*IP*) on average:

$$IP = \frac{1}{100}\sum_{i=1}^{100}\left|\frac{MD_i}{md_i}\right| \quad (14)$$

Where *i* is the atomic number of elements, varying from 1 to 100, MD_i and md_i are the mean absolute relative difference value of the *i*-th element for Geant4 10.6 and 11.0 respectively, calculated using equation (13).

We obtained an *IP* about 1.3.

3. Comparative study of Geant4 photon models with respect to the XCOM data library

3.1. Method

The comparative study described in this section concerns the comparison of the mass attenuation coefficient for selected elements and compounds with respect to the XCOM reference database from National Institute of Standards and Technology (NIST) (*https://www.nist.gov/pml/xcom-photon-cross-sections-database*). We chose beryllium, carbon, aluminum, silicon, germanium, iron, silver, cesium, gold, lead, uranium, water and ICRU compact bone [47] to sample a broad spectrum of materials. For this, we followed the procedure described by Amako *et al*. [32], which is also used by the G4-Med benchmarking system for medical physics [33]. We considered a monoenergetic photon beam (point source, number of incident photons N_0) passing through a homogeneous slab, with a given thickness, density and composition, made of one of the selected elements or materials above. 50 energy values varying from 1 keV to 100 GeV were tested. The choice of tested energies corresponds to the available data provided by XCOM. In this study, we aimed to compare the mass attenuation coefficient for both total photon interaction μ_m and each process $(\mu_m)_p$ using photon models in Geant4 10.6 and 11.0.

The total mass attenuation coefficient μ_m is calculated as follows:

$$\mu_m = \frac{1}{\rho d} ln\left(\frac{N_0}{N}\right) \quad (15)$$

where ρ represents the density (g/cm^3) of the slab and and d its thickness. N_0 is the number of incident photons, N is the number of photons traversing the slab without interacting, which was obtained from the Geant4 simulation.

The partial mass attenuation coefficient $(\mu_m)_p$ is calculated using the following equation:

$$(\mu_m)_p = \frac{(\mu_l)_p}{\rho} \quad (16)$$

where $(\mu_l)_p$ is the linear attenuation coefficient for a single process p. The value of $(\mu_l)_p$ was calculated by the Geant4 simulation.

3.2. Simulation uncertainty

In our case, the statistical simulation uncertainty σ_{μ_m} is expressed as:

$$\sigma_{\mu_m} = \sqrt{\left(\frac{1}{\rho d}\right)^2 \frac{1}{N}} \quad (17)$$

The calculation of the statistical uncertainty is detailed in Appendix A, equations (A1) - (A6). In order to minimize the uncertainty, a higher number of incident photons (N_0 = 10^6) was taken compared to the study of Amako *et al*. [32] (using 10^4 photons). Moreover, the thickness d of the slab was adjusted so as to have a sufficient number of photons, N, that did not interact with the slab. In this way, we ensured that the relative uncertainty on the attenuation coefficient $\frac{\sigma_{\mu_m}}{\mu_m}$ was always less than 0.3%.

3.3. Results

The mass attenuation coefficients were calculated with Geant4 simulations for water (Fig. B11) and all the other selected materials. The relative difference in percentage was also calculated with respect to XCOM using the following equation:

$$\text{Relative difference (\%)} = \frac{\text{Simulation} - \text{XCOM}}{\text{XCOM}} \times 100 \quad (18)$$

Thus, the maximal relative difference for the selected materials is shown as a function of Z in Fig. B12. We observed that for the selected elements and compounds, the maximal relative difference for Geant4 11.0 is of the same order of magnitude for Geant4 10.6. For the total attenuation coefficient, the maximal relative difference is less than 4.5% in absolute value for both Geant4 10.6 and 11.0, except for cesium, which is about -12% for Geant4 11.0, in contrast with -1.2% for Geant4 10.6. This variation between Geant4 10.6 and 11.0 results from the difference of cross-section of the photoelectric effect at 1 keV, which is exactly the energy of cesium where an abrupt variation of the cross-sections occurs (Fig. B13). The maximal relative difference for other processes is similar for Geant4 11.0 and 10.6 compared to XCOM: less than 0.045% in absolute value for gamma conversion, 4.7% for Compton scattering, and 64% for Rayleigh scattering. As discussed before, because the maximal difference is not always representative due to outliers, we plotted the mean absolute relative difference (*MD*) as a function of Z (Fig. 7). The *MD* was calculated according to the equation (13) with m, the number of tested energy points for a given material, r_i, the relative difference of the i-th energy point, expressed as equation (18). When compared to XCOM, the *MD* for both Geant4 10.6 and 11.0 are similar: less than 0.49% for total, 0.015% for gamma conversion, 1.3% for Compton scattering, 0.67%

for photoelectric and 17% for Rayleigh scattering. We can notice that for Geant4 11.0 and 10.6, large differences were observed at low energies below 100 keV for Rayleigh scattering when compared to XCOM, *e.g.* 64% for maximal relative difference and 17% for *MD*. Nevertheless, the photoelectric effect dominates in the 100 eV - 100 keV energy range. Thus, the impact of Rayleigh scattering on the precision of the total cross-section is negligible compared to the photoelectric effect.

3.4. Discussion

In the present study, we used the maximal and mean absolute relative difference to quantitatively compare our simulation results with the XCOM data in order to evaluate our implemented models. However, from the literature, we noticed that many researchers used statistical analysis based on goodness of fit testing to assess the accuracy of their models, in terms of either total mass attenuation coefficient or partial interaction coefficient, with respect to a reference database [31, 32, 48-51]. A χ^2 test was performed and a confidence level (p-value) was set at a defined value (generally 0.05 or 0.01). The calculation of χ^2 takes into account the data uncertainties [52] , as follows:

$$\chi^2 = \sum_{i=1}^{n} \frac{(O_i - E_i)^2}{{\sigma_i}^2} \quad (19)$$

where *n* is the number of points, O_i the *i*-th observed value, from simulation, E_i the expected value (reference data) and σ_i the uncertainty on observed values. σ_i consists of the statistical simulation uncertainty, and systematic uncertainty on cross-section data, which is not known precisely on the whole energy range [41].

An appropriate estimation of uncertainty σ_i is important, as it greatly affects the χ^2 score and corresponding p-value. However, we noticed that in these previous studies in the literature, the calculation of χ^2 only considered the statistical uncertainty as σ_i, while the systematic uncertainty on cross-section data was not taken into account. The χ^2 test was nevertheless consistent, because their statistical uncertainty was a few percent, which was roughly of the same order of magnitude as the cross section data uncertainties. In our case, as explained in section 3.2, our simulations were performed with a higher number of incident photons, which leads to a better statistical precision, less than 0.3%. It would not make sense if we calculated χ^2 using our statistical uncertainty as σ_i, because it is not representative of the real total uncertainty, which is now dominated by the systematic uncertainty of the cross-section data. Therefore, we did not take into account the χ^2 test to evaluate our implemented models in the present work, but rather used maximal and mean absolute relative difference.

A second point that we would like to address here is the CPU time variation between Geant4 10.6 and the updated models. Since our new parameterizations are based on the same type of fitting functions as Geant4 10.6, the simulations made with updated models are expected to have a similar CPU time performance. This was verified by simulations with different elements and different incident photon energies.

4. Conclusions

In this work, we have presented in detail the implementation of EPICS2017 database for Geant4 Livermore photon models included in Geant4 11.0 release. We updated data relevant to four photon processes: i) Gamma conversion: cross-sections; ii) Compton scattering: cross-sections and scattering functions; iii) Photoelectric effect: cross-sections; iv) Rayleigh scattering: cross-sections and form factors. The parameterizations used in Geant4 10.6 were updated in order to be suited to EPICS2017

data. The relative differences of the fitted values with respect to the tabulated values were quantitatively investigated for updated parameterizations, and then compared with those for the parameterizations in Geant4 10.6. The precision of these updated parameterizations was improved compared to Geant4 10.6, by a factor of roughly: 1000 for region 1 and 2.8 for region 2 of Compton scattering functions (scattering functions were fitted in two intervals). As previously discussed, the factor of 1000 does not mean the parameterizations in Geant4 10.6 were bad as the individual differences were relatively small (5-10%) and the region of difference is for low momentum transfer. For the photoelectric effect, the precision of the updated parameterization was improved by a factor of 1.9 for low energy region and 1.3 for high energy region of total cross-sections (also fitted in two intervals); and by a factor of 1.3 for form factors of Rayleigh scattering. The rest of data were directly tabulated in Geant4. Geant4 reads the tabulated data and does its own interpolation to calculate the cross-section at a given energy point. The way Geant4 interpolates, depends on the nature of the data that Geant4 reads. Considering that EPICS2017 uses linear interpolation, thus it had to be also applied in Geant4 11.0 models, while Geant4 10.6 used logarithmic interpolation, which was implemented in EPDL97.

The updated models were tested through a comparative study regarding mass attenuation coefficients. The mass attenuation coefficients for total and each process were calculated with Geant4 11.0 and 10.6, respectively, for selected elements and compounds. A good agreement with XCOM data was observed, except for Rayleigh scattering below 100 keV. However in this energy range, the photoelectric effect dominates, so there is little impact on the precision of total mass attenuation coefficient. The mean absolute relative difference of total mass attenuation coefficients between simulation results, using both Geant4 10.6 and 11.0, and XCOM data does not exceed 0.49%. This comparison thus confirms the very good agreement between the simulation results obtained with Geant4 11.0 and XCOM data.

Acknowledgements

The authors would also like to thank the Geant4 collaboration for their technical support and advice. This work has been financially supported by China Scholarship Council, through a four-year funding of Z. Li's PhD at University of Bordeaux, France. We also thank CNRS/IN2P3 for providing support to the Geant4 project (*http://geant4.in2p3.fr*).

Reference

[1] Agostinelli S, Allison J, Amako Ka, Apostolakis J, Araujo H, Arce P, et al. GEANT4—a simulation toolkit. Nucl Instrum Methods Phys Res A. 2003;506:250-303.
[2] Allison J, Amako K, Apostolakis J, Araujo H, Arce Dubois P, Asai M, et al. Geant4 developments and applications. IEEE Trans Nucl Sci. 2006;53:270-8.
[3] Allison J, Amako K, Apostolakis J, Arce P, Asai M, Aso T, et al. Recent developments in Geant4. Nucl Instrum Methods Phys Res A. 2016;835:186-225.
[4] Ivanchenko V, Apostolakis J, Bagulya A, Abdelouahed HB, Black R, Bogdanov A, et al. Recent Improvements in Geant4 Electromagnetic Physics Models and Interfaces. Prog Nucl Sci Technol. 2011;2:898-903.
[5] Ivanchenko V, Incerti S, Allison J, Bagulya A, Brown J, Champion C, et al., editors. Geant4 electromagnetic physics: improving simulation performance and accuracy. SNA+ MC 2013-Joint International Conference on Supercomputing in Nuclear Applications+ Monte Carlo; 2014: EDP Sciences.
[6] Salvat F, editor PENELOPE-2018: A Code System for Monte Carlo Simulation of Electron and Photon Transport. Workshop Proceedings 2019; Barcelona, Spain.

[7] Cullen D, Hubbell JH, Kissel L. The Evaluated Photon Data Library 97 version. UCRL-50400. 1997;6.
[8] Perkins S, Cullen D, Seltzer S. Tables and graphs of electron-interaction cross-sections from 10 eV to 100 GeV derived from the LLNL evaluated electron data library (EEDL), Z= 1-100. UCRL-50400. 1991;31:21-4.
[9] Perkins S, Cullen D, Chen M, Rathkopf J, Scofield J, Hubbell J. Tables and graphs of atomic subshell and relaxation data derived from the LLNL Evaluated Atomic Data Library (EADL), Z= 1--100. Lawrence Livermore National Lab., CA (United States); 1991.
[10] Inguimbert C, Caron P, Gibaru Q, Sicard A, Balcon N, Ecoffet R. Surface ionizing dose for space applications estimated with low energy spectra going down to hundreds of eV. IEEE Trans Nucl Sci. 2020.
[11] Miceli A, Festa G, Gorini G, Senesi R, Andreani C. Pulsed neutron gamma-ray logging in archaeological site survey. Meas Sci Technol. 2013;24:125903.
[12] Poder J, Cutajar D, Guatelli S, Petasecca M, Howie A, Bucci J, et al. HDR brachytherapy in vivo source position verification using a 2D diode array: A Monte Carlo study. J Appl Clin Med Phys. 2018;19:163-72.
[13] Pope DJ, Cutajar DL, George SP, Guatelli S, Bucci JA, Enari KE, et al. The investigation of prostatic calcifications using μ-PIXE analysis and their dosimetric effect in low dose rate brachytherapy treatments using Geant4. Phys Med Biol. 2015;60:4335-53.
[14] Lazarakis P, Incerti S, Ivanchenko V, Kyriakou I, Emfietzoglou D, Corde S, et al. Investigation of track structure and condensed history physics models for applications in radiation dosimetry on a micro and nano scale in Geant4. Biomed Phys Eng Express. 2018;4:024001.
[15] Liu R, Higley KA, Swat MH, Chaplain MAJ, Powathil GG, Glazier JA. Development of a coupled simulation toolkit for computational radiation biology based on Geant4 and CompuCell3D. Phys Med Biol. 2021;66:045026.
[16] Michelet C, Li Z, Yang W, Incerti S, Desbarats P, Giovannelli JF, et al. A Geant4 simulation for three-dimensional proton imaging of microscopic samples. Phys Med. 2019;65:172-80.
[17] Beaudoux V, Blin G, Barbrel B, Kantor G, Zacharatou C. Geant4 physics list comparison for the simulation of phase-contrast mammography (XPulse project). Phys Med. 2019;60:66-75.
[18] Incerti S, Barberet P, Dévès G, Michelet C, Francis Z, Ivantchenko V, et al. Comparison of experimental proton-induced fluorescence spectra for a selection of thin high-Z samples with Geant4 Monte Carlo simulations. Nucl Instrum Methods Phys Res B. 2015;358:210-22.
[19] Cebastien Joel GS, Maurice NM, Eric Jilbert NM, Ousmanou M, David S. Monte Carlo method for gamma spectrometry based on GEANT4 toolkit: Efficiency calibration of BE6530 detector. J Environ Radioact. 2018;189:109-19.
[20] Sakata D, Belov O, Bordage M-C, Emfietzoglou D, Guatelli S, Inaniwa T, et al. Fully integrated Monte Carlo simulation for evaluating radiation induced DNA damage and subsequent repair using Geant4-DNA. Sci Rep. 2020;10:1-13.
[21] Incerti S, Baldacchino G, Bernal M, Capra R, Champion C, Francis Z, et al. The Geant4-DNA project. Int J Model Simul Sci Comput. 2010;1:157-78.
[22] Incerti S, Ivanchenko A, Karamitros M, Mantero A, Moretto P, Tran H, et al. Comparison of GEANT4 very low energy cross section models with experimental data in water. Med Phys. 2010;37:4692-708.
[23] Bernal M, Bordage M, Brown J, Davídková M, Delage E, El Bitar Z, et al. Track structure modeling in liquid water: A review of the Geant4-DNA very low energy extension of the Geant4 Monte Carlo simulation toolkit. Phys Med. 2015;31:861-74.
[24] Incerti S, Kyriakou I, Bernal M, Bordage M-C, Francis Z, Guatelli S, et al. Geant4‐DNA example applications for track structure simulations in liquid water: A report from the Geant4‐DNA Project. Med Phys. 2018;45:e722-e39.
[25] Schuemann J, McNamara AL, Ramos-Mendez J, Perl J, Held KD, Paganetti H, et al. TOPAS-nBio: An Extension to the TOPAS Simulation Toolkit for Cellular and Sub-cellular Radiobiology. Radiat Res. 2019;191:125-38.

[26] Faddegon B, Ramos-Mendez J, Schuemann J, McNamara A, Shin J, Perl J, et al. The TOPAS tool for particle simulation, a Monte Carlo simulation tool for physics, biology and clinical research. Phys Med. 2020;72:114-21.
[27] Pham QT, Anne A, Bony M, Delage E, Donnarieix D, Dufaure A, et al. Coupling of Geant4-DNA physics models into the GATE Monte Carlo platform: Evaluation of radiation-induced damage for clinical and preclinical radiation therapy beams. Nucl Instrum Methods Phys Res B. 2015;353:46-55.
[28] Costa GCA, Sa LVd, Bonifacio DAB. Application of GATE/Geant4 for internal dosimetry using male ICRP reference voxel phantom by specific absorbed fractions calculations for photon irradiation. Biomed Phys Eng Express. 2015;1.
[29] Arce P, Lagares JI, Harkness L, Desorgher L, De Lorenzo G, Abreu Y, et al., editors. GAMOS: an easy and flexible way to use GEANT4. 2011 IEEE Nuclear Science Symposium Conference Record; 2011: IEEE.
[30] Dubois PA, Thao NTP, Nguyen TT, Azcona JD, Aguilar-Redondo P-B. A tool for precise calculation of organ doses in voxelised geometries using GAMOS/Geant4 with a graphical user interface. Pol J Med Phys. 2021;27:31-40.
[31] Cirrone GAP, Cuttone G, Di Rosa F, Pandola L, Romano F, Zhang Q. Validation of the Geant4 electromagnetic photon cross-sections for elements and compounds. Nucl Instrum Methods Phys Res A. 2010;618:315-22.
[32] Amako K, Guatelli S, Ivanchenko VN, Maire M, Mascialino B, Murakami K, et al. Comparison of Geant4 electromagnetic physics models against the NIST reference data. IEEE Trans Nucl Sci. 2005;52:910-8.
[33] Arce P, Bolst D, Bordage MC, Brown J, Cirrone P, Cortés-Giraldo M, et al. Report on G4-Med, a Geant4 benchmarking system for medical physics applications developed by the Geant4 Medical Simulation Benchmarking Group. Med Phys. 2021;48:19-56.
[34] Berger MJ, Hubbell J. XCOM: Photon cross sections on a personal computer. National Bureau of Standards, Washington, DC (USA). Center for Radiation; 1987.
[35] Biggs F, Lighthill R. Analytical approximations for x-ray cross sections III. Sandia National Labs., Albuquerque, NM (USA); 1988. p. 137.
[36] Poon E, Verhaegen F. Medical physics community Accuracy of the photon and electron physics in GEANT4 for radiotherapy applications. Med Phys. 2005;32:1696-711.
[37] Medhat ME, Singh VP. Mass attenuation coefficients of composite materials by Geant4, XCOM and experimental data: comparative study. Radiat Eff Defects Solids. 2014;169:800-7.
[38] Obaid SS, Sayyed MI, Gaikwad DK, Tekin HO, Elmahroug Y, Pawar PP. Photon attenuation coefficients of different rock samples using MCNPX, Geant4 simulation codes and experimental results: a comparison study. Radiat Eff Defects Solids. 2018;173:900-14.
[39] Al-Buriahi MS, Arslan H, Tonguç BT. Mass attenuation coefficients, water and tissue equivalence properties of some tissues by Geant4, XCOM and experimental data. Indian J Pure Appl Phys. 2019;57:433-7.
[40] Cullen DE. EPICS2017: April 2019 status report. NA; 2019.
[41] Cullen DE. A survey of photon cross section data for use in EPICS2017. IAEA-NDS-225, rev. 1; 2018.
[42] Doglioni C, Ivanchenko V, Bagulya A, Bakr S, Bandieramonte M, Bernard D, et al. Geant4 electromagnetic physics progress. EPJ Web of Conferences. 2020;245.
[43] Hubbell JH. Summary of existing information on the incoherent scattering of photons, particularly on the validity of the use of the incoherent scattering function. Radiat Phys Chem. 1997;50:113-24.
[44] Cullen DE. A simple model of photon transport. Nucl Instrum Methods Phys Res B. 1995;101:499-510.
[45] Hubbell JH, Overbo I. Relativistic atomic form factors and photon coherent scattering cross sections. J Phys Chem Ref Data. 1979;8:69-106.
[46] Batic M, Hoff G, Pia MG, Saracco P. Photon Elastic Scattering Simulation: Validation and Improvements to Geant4. IEEE Trans Nucl Sci. 2012;59:1636-64.
[47] Report 10b. J ICRU. 1964;os6:NP-NP.

[48] Weidenspointner G, Batic M, Hauf S, Hoff G, Kuster M, Pia MG, et al., editors. Validation of Compton scattering Monte Carlo simulation models. 2013 IEEE Nuclear Science Symposium and Medical Imaging Conference (2013 NSS/MIC); 2013: IEEE.
[49] Guatelli S, Mascialino B, Pia M, Piergentili M, Pandola L, Parlati S, et al., editors. Precision validation of Geant4 electromagnetic physics. American Nuclear Society Topical Meeting in Monte Carlo; 2005.
[50] Amako K, Guatelli S, Ivanchencko V, Maire M, Mascialino B, Murakami K, et al., editors. Validation of Geant4 electromagnetic physics versus protocol data. IEEE Symposium Conference Record Nuclear Science 2004; 2004.
[51] Marcia Begalli GH, Maria Grazia Pia, Paolo G. Saracco, editor Validation of Geant4 Electron Pair Production by Photons. 2013 IEEE Nuclear Science Symposium and Medical Imaging Conference; 2013.
[52] Cirrone G, Donadio S, Guatelli S, Mantero A, Mascialino B, Parlati S, et al. A goodness-of-fit statistical toolkit. IEEE Trans Nucl Sci. 2004;51:2056-63.

Appendix A: simulation uncertainty on the mass attenuation coefficient

$$\mu_m = \frac{1}{\rho d} ln\left(\frac{N_0}{N}\right) \qquad (A1)$$

$$\sigma_{\mu_m} = \sqrt{\left(\frac{d\mu_m}{dN}\right)^2 {\sigma_N}^2} \quad (A2)$$

Considering:

$$\frac{d\mu_m}{dN} = -\frac{1}{\rho dN} \qquad (A3)$$

And the uncertainty on the number of detected photons *N*:

$$\sigma_N = \sqrt{N} \qquad (A4)$$

Thus:

$$\sigma_{\mu_m} = \sqrt{\left(\frac{1}{\rho d}\right)^2 \left(\frac{{\sigma_N}^2}{N^2}\right)} = \sqrt{\left(\frac{1}{\rho d}\right)^2 \frac{1}{N}} \qquad (A5)$$

Finally, relative uncertainty $\frac{\sigma_{\mu m}}{\mu_m}$ was obtained as follows:

$$\frac{\sigma_{\mu_m}}{\mu_m} = \frac{\sqrt{\left(\frac{1}{\rho d}\right)^2 \frac{1}{N}}}{-\frac{1}{\rho d} ln\left(\frac{N}{N_0}\right)} = \frac{1}{ln\left(\frac{N_0}{N}\right)} \sqrt{\frac{1}{N}} \qquad (A6)$$

Appendix B: Supplementary figures

Figure captions

Figures should all be in black and white in the printed version

Fig. 1. Regions and sub-regions for the fits of scattering functions of Compton effect. The top figure represents the regions for Geant4 10.6, the bottom for Geant4 11.0.

Fig. 2. Maximal relative difference of fitted scattering functions of Compton effect as a function of atomic number (Z: 1-100) in region 1 (left) and region 2 (right), for Geant4 11.0 (open circles) and Geant4 10.6 (filled squares). The relative difference is calculated by equation (4).

Fig. 3. Maximal relative difference (open circles) and mean absolute relative difference value (filled squares) in binding energies of EPICS2017 compared to EPDL97 as a function of atomic number (Z: 1-100). The relative difference and mean absolute relative difference are calculated by equation (6) and (7) respectively.

Fig. 4. Regions for the calculation of cross-sections of the photoelectric effect: EB_K is the binding energy of K-shell; E_a is the low energy limit; E_b is the high energy limit.

Fig. 5. Maximal relative difference in low (left) and high energy fit (right) of total cross-sections of the photoelectric effect as a function of atomic number (Z: 1-100), for Geant4 11.0 (open circles) and Geant4 10.6 (filled squares). The relative difference is calculated by equation (4).

Fig. 6. Mean absolute relative difference in fitted square of form factors of Rayleigh scattering compared to tabulated data as a function of atomic number (Z: 1-100), for Geant4 11.0 (open circles) and Geant4 10.6 (filled squares). The relative difference is calculated by equation (12).

Fig. 7. Mean absolute relative difference in mass attenuation coefficients as a function of atomic number, for Geant4 11.0 (open circles for the selected chemical elements, cross + for compound materials) and 10.6 (filled squares for the selected chemical elements, cross × for compound materials) compared to XCOM, for total and each process. The values for the selected compound materials are represented according to their effective atomic number: 3.3 for water and 4.4 for ICRU compact bone. The calculation of relative difference and mean absolute relative difference is explained in section 3.3.

Figure captions for Appendix B

Fig. B1. Cross-sections of gamma conversion as a function of energy, for hydrogen (Z = 1), aluminum (Z = 13) and lead (Z = 82), for pair (left) and triplet (right) production, from EPICS2017 (open circles), EPDL97 (filled squares).

Fig. B2. Cross-sections of as a function of energy (left) and scattering functions as a function of momentum transfer (right) of Compton scattering from EPICS2017 (open circles), EPDL97 (filled squares).

Fig. B3. Relative difference in fitted scattering functions of Compton effect as a function of momentum transfer for Geant4 11.0 (open circles) and 10.6 (filled squares). The relative difference is calculated by equation (4). The lines are used only to guide the eye.

Fig. B4. Binding energies (left) from EPICS2017 (open circles) and EPDL97 (filled squares). Relative difference in binding energies of EPICS2017 (right) compared to EPDL97 (equation (6)).

Fig. B5. Total cross-sections (left) of the photoelectric effect as a function of energy from EPICS2017 (open circles) and EPDL97 (filled squares). Relative difference EPICS2017 (right) compared to EPDL97 (equation (6)).

Fig. B6. Fitted K shell cross-sections of the photoelectric effect (left) as a function of energy for Geant4 11.0: low energy fit (filled squares), high energy fit (open circles), tabulated EPICS2017 (points). Relative difference (right) compared to tabulated values (equation (4)).

Fig. B7. Maximal relative difference in low energy fit (left) and high energy fit (right) of subshell cross-sections of the photoelectric effect, as a function of atomic number (Z: 1-100), for Geant4 11.0 (open circles) and 10.6 (filled squares). The relative difference is calculated by equation (4).

Fig. B8. Mean absolute relative difference in low energy fit (left) and high energy fit (right) of subshell cross-sections of the photoelectric effect, as a function of atomic number (Z: 1-100), for Geant4 11.0 (open circles) and 10.6 (filled squares). The mean absolute relative difference is calculated by equation (10).

Fig. B9. Cross-sections as a function of energy (left) and form factors as a function of momentum transfer (right) of Rayleigh scattering, for hydrogen, aluminum and lead, from EPICS2017 (open circles), EPDL97 (filled squares).

Fig. B10. Relative difference in fitted form factors of Rayleigh scattering as a function of momentum transfer, for Geant4 11.0 (open circles) and 10.6 (filled squares). The relative difference is calculated by equation (12).

Fig. B11 (*2 pages*). Mass attenuation coefficient for water as a function of energy (left), for Geant4 11.0 (open circles) and 10.6 (filled squares) as well as XCOM data (filled triangles). Relative difference (right) compared to the XCOM database, for total and each process (equation (18)).

Fig. B12. Maximal relative difference in mass attenuation coefficients as a function of atomic number, for Geant4 11.0 (open circles for the selected chemical elements, cross + for compound materials) and 10.6 (filled squares for the selected chemical elements, cross × for compound materials) compared to XCOM, for total and each process. The values for the selected compound materials are represented according to their effective atomic number: 3.3 for water and 4.4 for ICRU compact bone. The relative difference is calculated by equation (18).

Fig. B13. Mass attenuation coefficient of the photoelectric effect for cesium as a function of energy (left), calculated by Geant4 11.0 (open circles) and 10.6 (filled squares) as well as XCOM data (filled triangles). Relative difference (right) compared to the XCOM database (equation (18)). The largest relative difference at 1 keV is clearly visible (arrow).

Fig.1

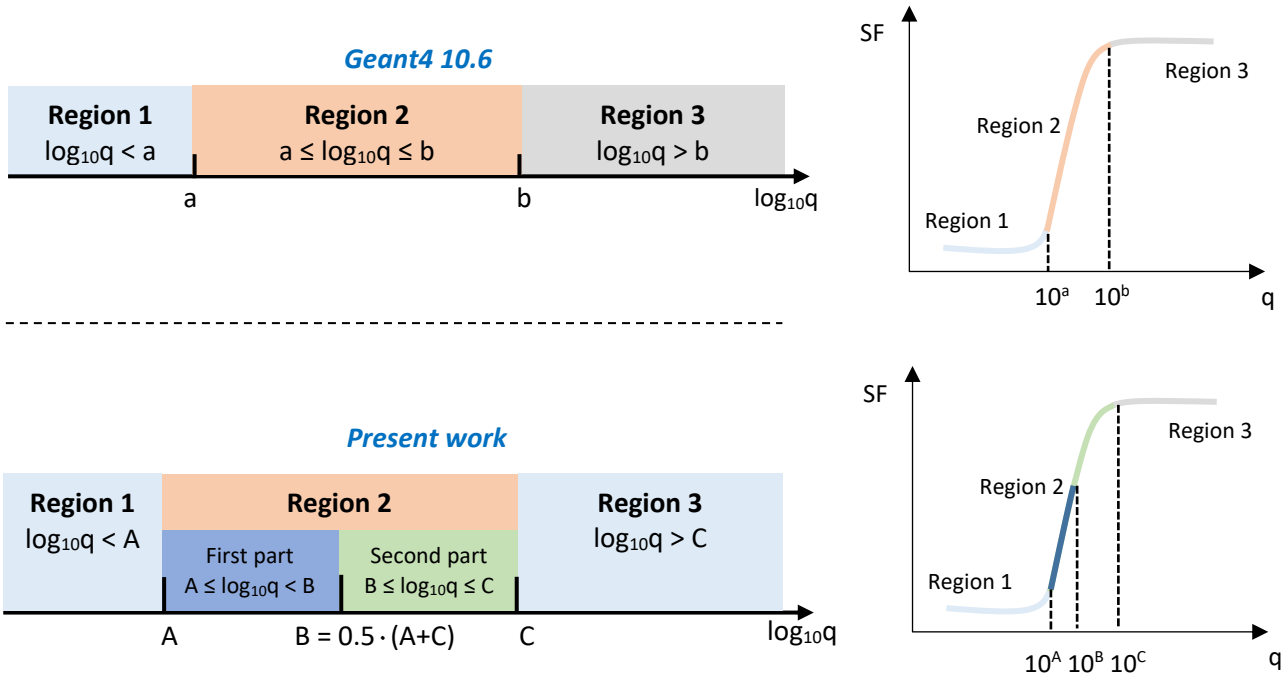
Geant4 10.6
Region 1
log10q < a
Region 2
a ≤ log10q ≤ b
Region 3
log10q > b
a
b
log10q
SF
Region 3
Region 2
Region 1
10a
10b
q
Present work
Region 1
log10q < A
Region 2
First part
A ≤ log10q < B
Second part
B ≤ log10q ≤ C
Region 3
log10q > C
A
B = 0.5 · (A+C)
C
log10q
SF
Region 3
Region 2
Region 1
10A 10B 10C
q

Fig.2

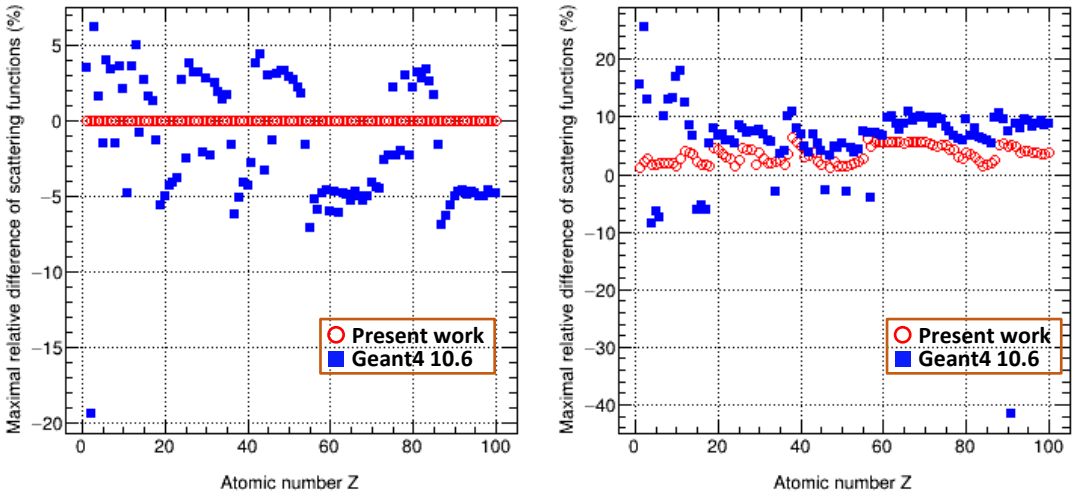
Maximal relative difference of scattering functions (%)
Atomic number Z
Present work
Geant4 10.6
Maximal relative difference of scattering functions (%)
Atomic number Z
Present work
Geant4 10.6

Fig.3

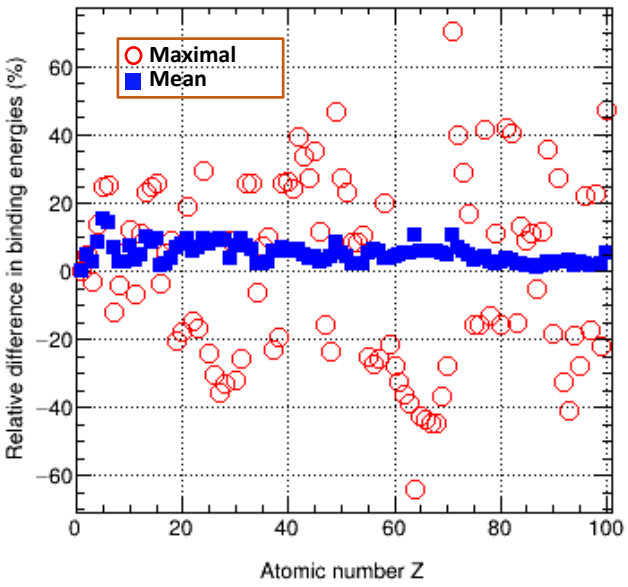
Maximal
Mean
Relative difference in binding energies (%)
60
40
20
0
−20
−40
−60
0
20
40
60
80
100
Atomic number Z

Fig.4

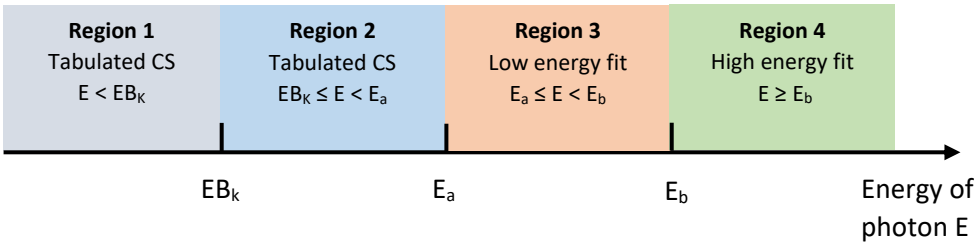
Region 1
Tabulated CS
E < EBK
Region 2
Tabulated CS
EBK ≤ E < Ea
Region 3
Low energy fit
Ea ≤ E < Eb
Region 4
High energy fit
E ≥ Eb
EBk
Ea
Eb
Energy of photon E

Fig.5

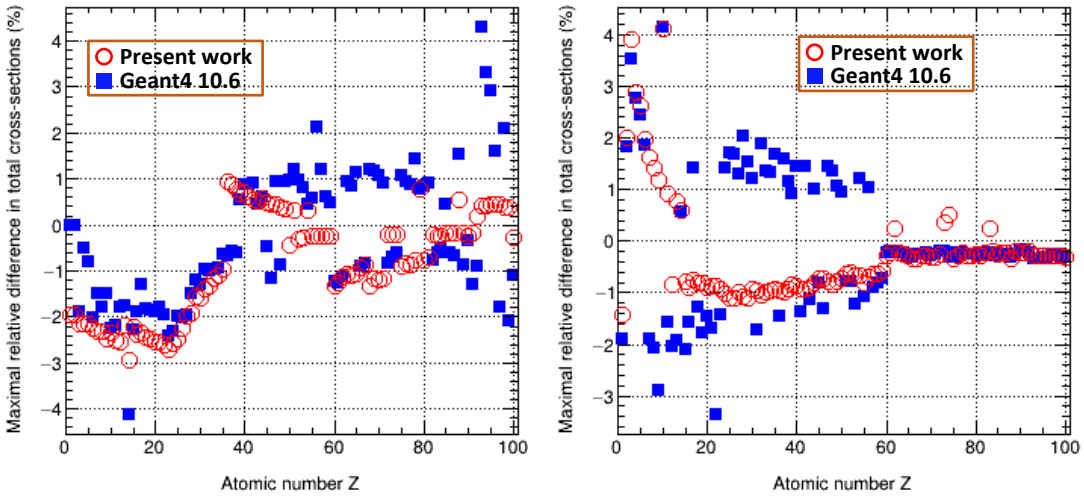
Present work
Geant4 10.6
Maximal relative difference in total cross-sections (%)
Atomic number Z
Present work
Geant4 10.6
Maximal relative difference in total cross-sections (%)
Atomic number Z

Fig.6

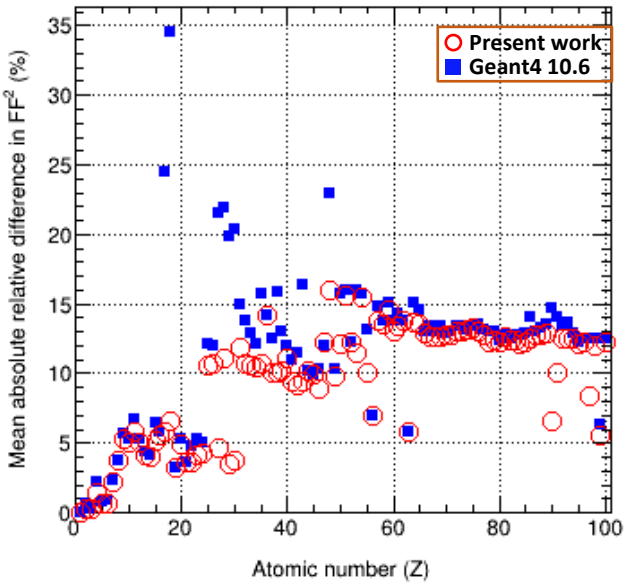
Present work
Geant4 10.6
Mean absolute relative difference in FF^2 (%)
Atomic number (Z)
0
5
10
15
20
25
30
35
0
20
40
60
80
100

Fig.7

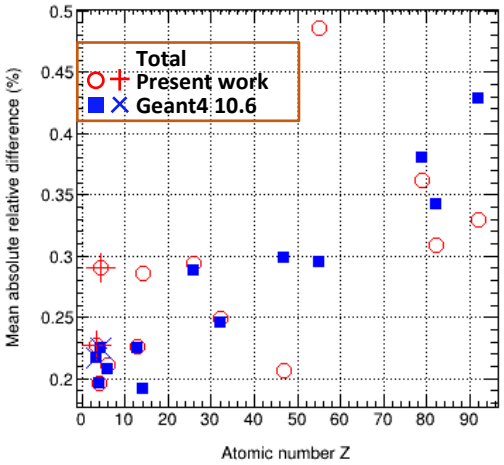
Total
Present work
Geant4 10.6
Mean absolute relative difference (%)
Atomic number Z

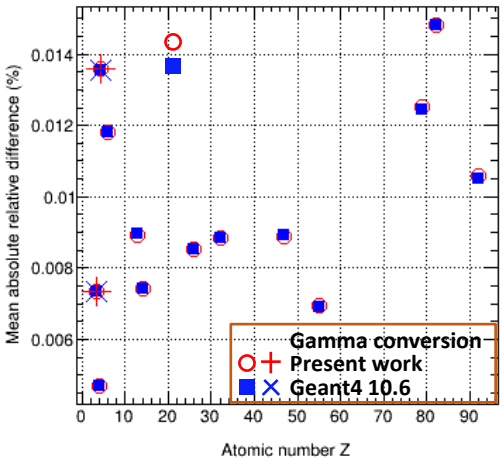
Gamma conversion
Present work
Geant4 10.6
Mean absolute relative difference (%)
Atomic number Z

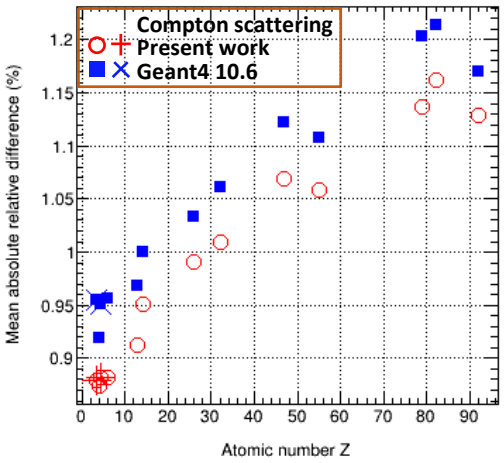
Compton scattering
Present work
Geant4 10.6
Mean absolute relative difference (%)
Atomic number Z

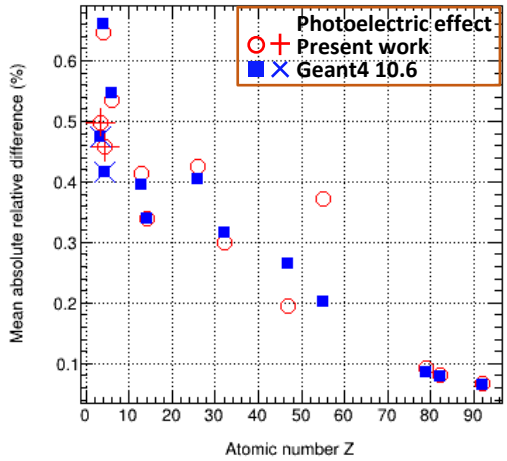
Photoelectric effect
Present work
Geant4 10.6
Mean absolute relative difference (%)
Atomic number Z

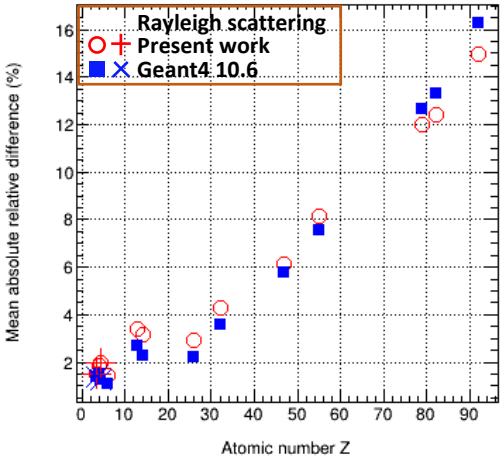
Rayleigh scattering
Present work
Geant4 10.6
Mean absolute relative difference (%)
Atomic number Z

FigB1

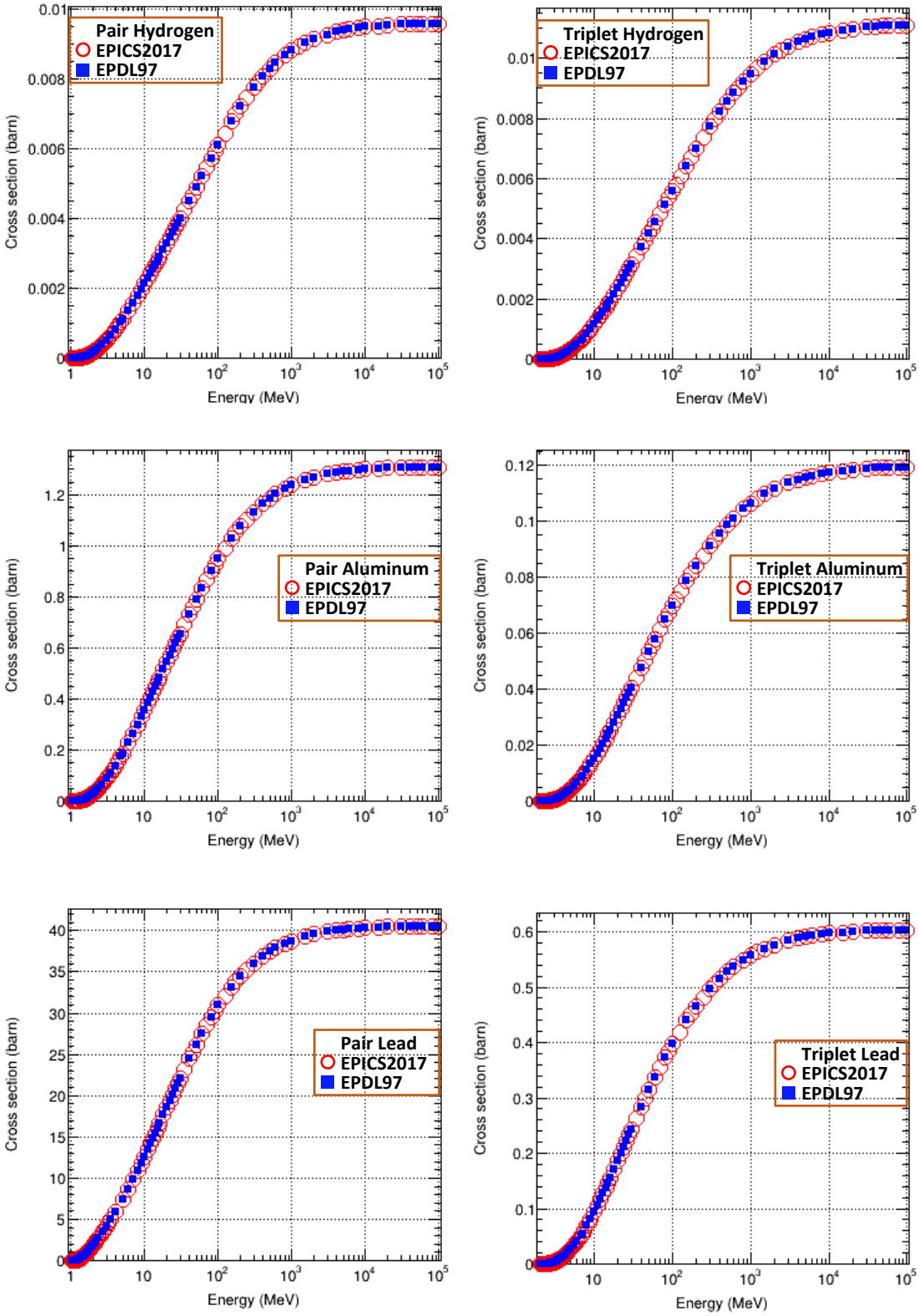
Pair Hydrogen
EPICS2017
EPDL97
Triplet Hydrogen
EPICS2017
EPDL97
Pair Aluminum
EPICS2017
EPDL97
Triplet Aluminum
EPICS2017
EPDL97
Pair Lead
EPICS2017
EPDL97
Triplet Lead
EPICS2017
EPDL97
Cross section (barn)
Energy (MeV)

FigB2

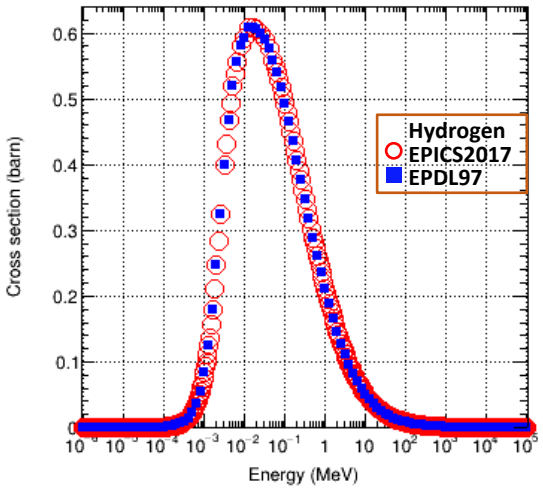
Cross section (barn)
Energy (MeV)
Hydrogen
EPICS2017
EPDL97

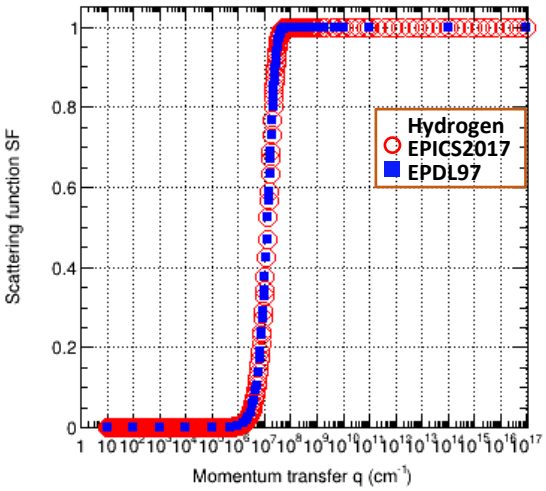
Scattering function SF
Momentum transfer q (cm-1)
Hydrogen
EPICS2017
EPDL97

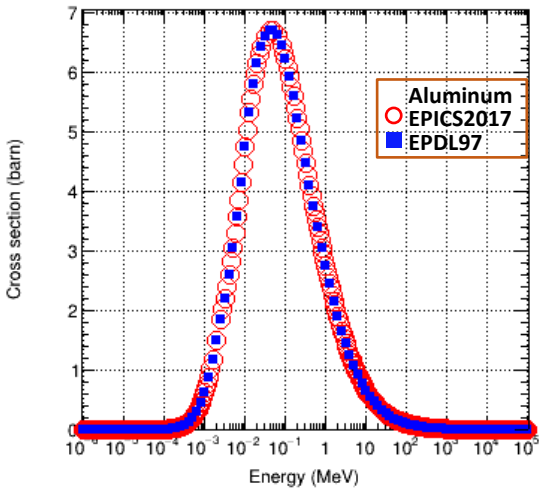
Cross section (barn)
Energy (MeV)
Aluminum
EPICS2017
EPDL97

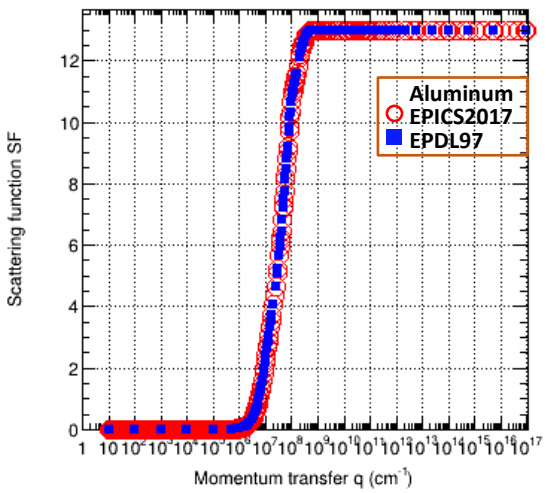
Scattering function SF
Momentum transfer q (cm-1)
Aluminum
EPICS2017
EPDL97

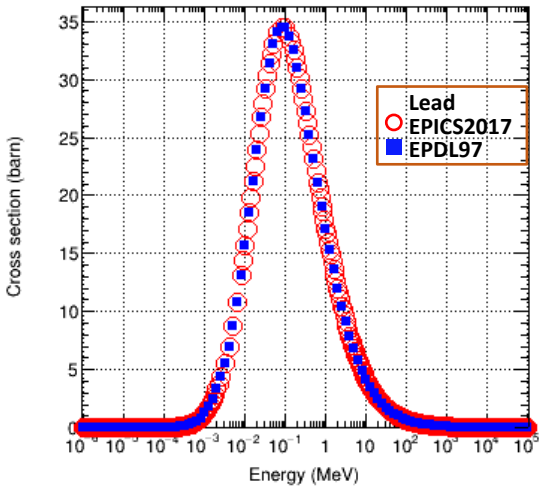
Cross section (barn)
Energy (MeV)
Lead
EPICS2017
EPDL97

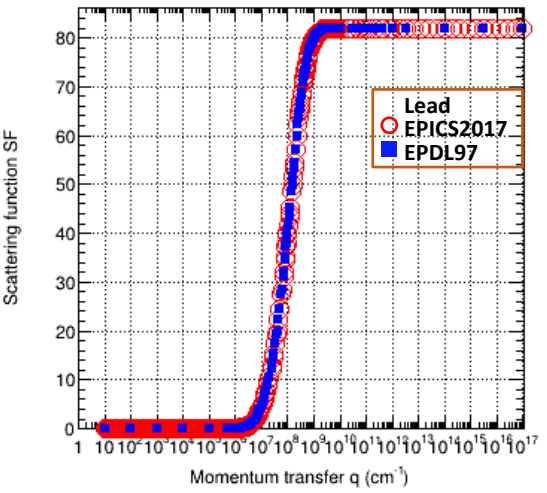
Scattering function SF
Momentum transfer q (cm-1)
Lead
EPICS2017
EPDL97

FigB3

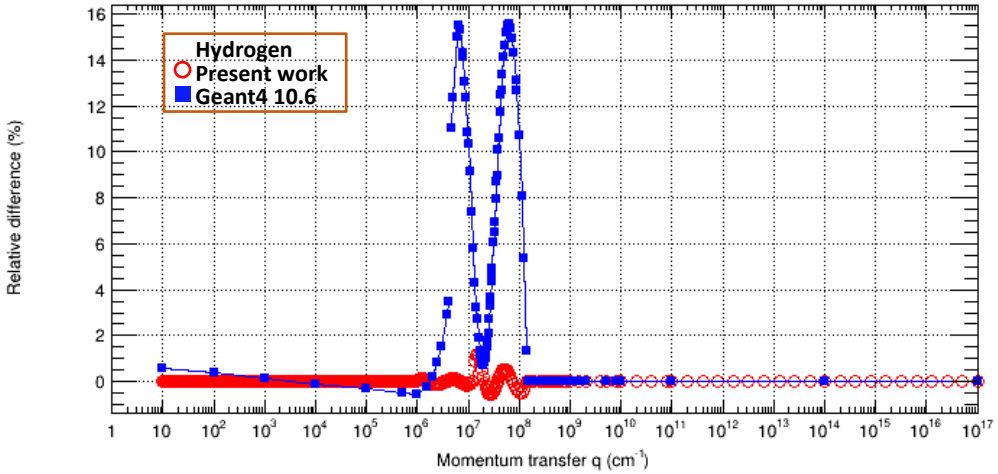
Hydrogen
Present work
Geant4 10.6
Relative difference (%)
Momentum transfer q (cm^{-1})

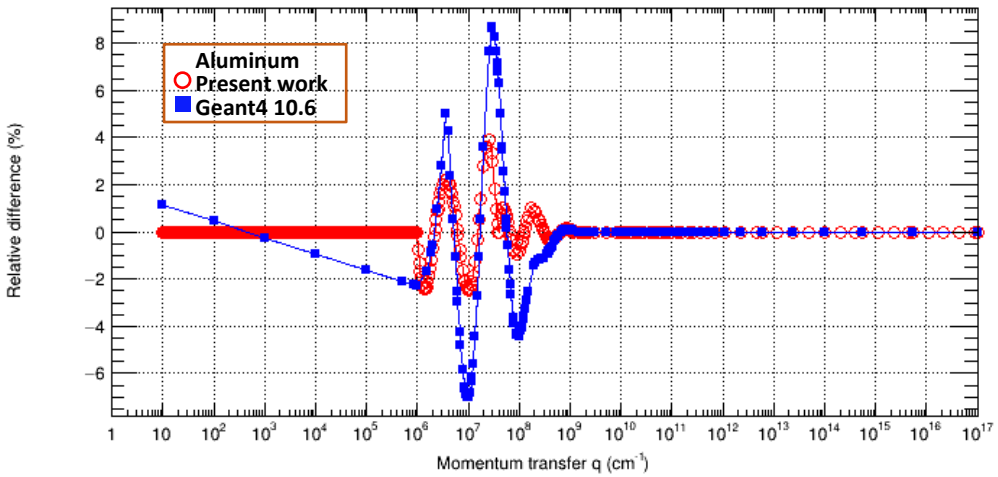
Aluminum
Present work
Geant4 10.6
Relative difference (%)
Momentum transfer q (cm^{-1})

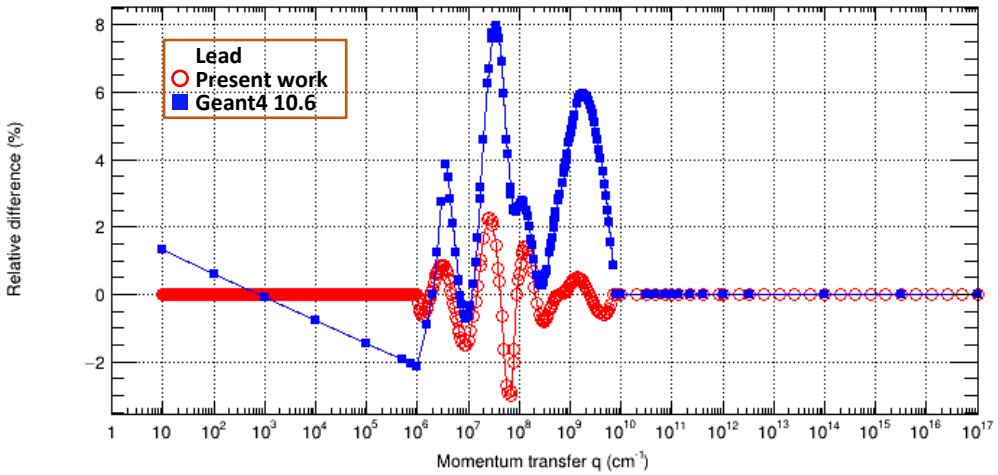
Lead
Present work
Geant4 10.6
Relative difference (%)
Momentum transfer q (cm^{-1})

FigB4

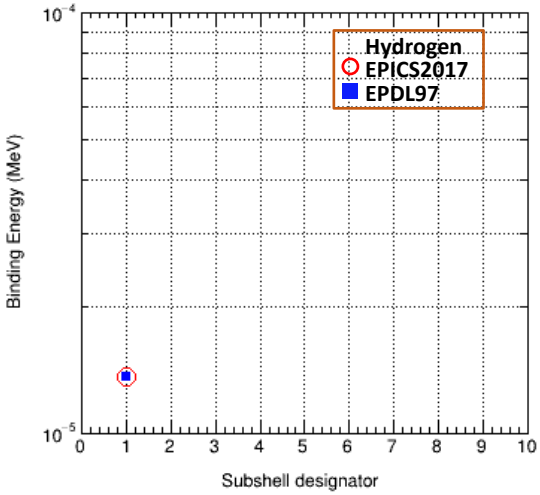
Hydrogen
EPICS2017
EPDL97
Binding Energy (MeV)
Subshell designator

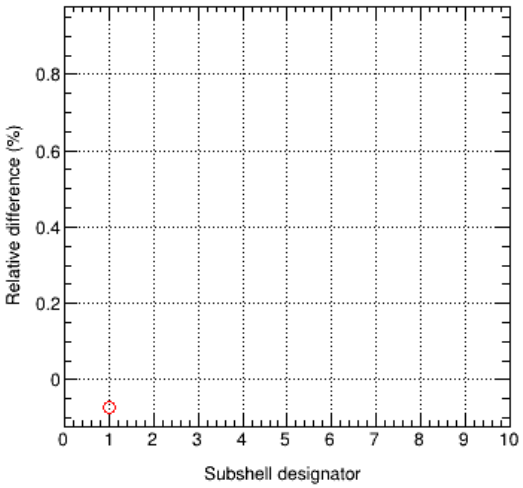
Relative difference (%)
Subshell designator

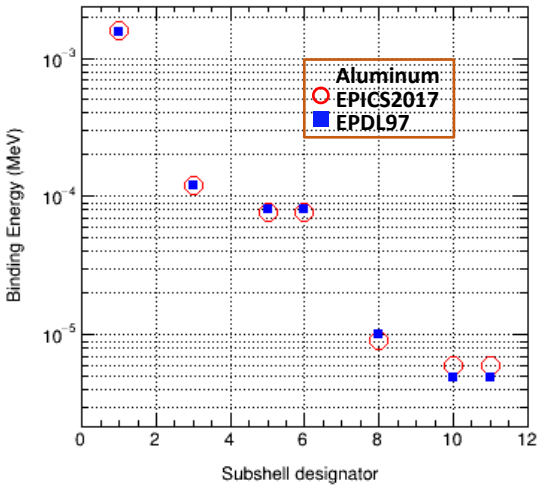
Aluminum
EPICS2017
EPDL97
Binding Energy (MeV)
Subshell designator

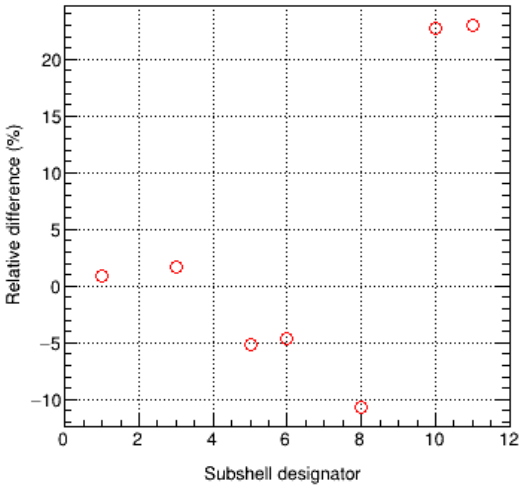
Relative difference (%)
Subshell designator

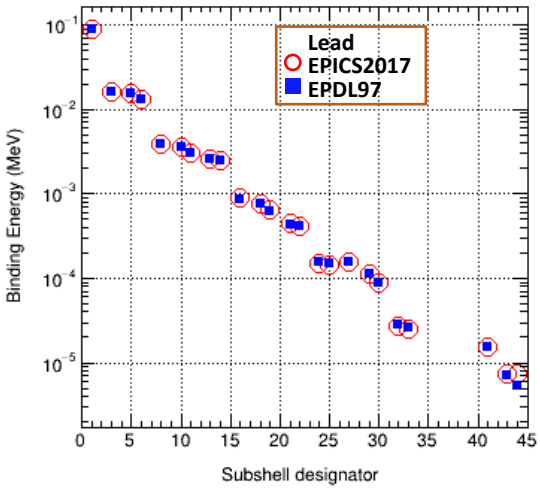
Lead
EPICS2017
EPDL97
Binding Energy (MeV)
Subshell designator

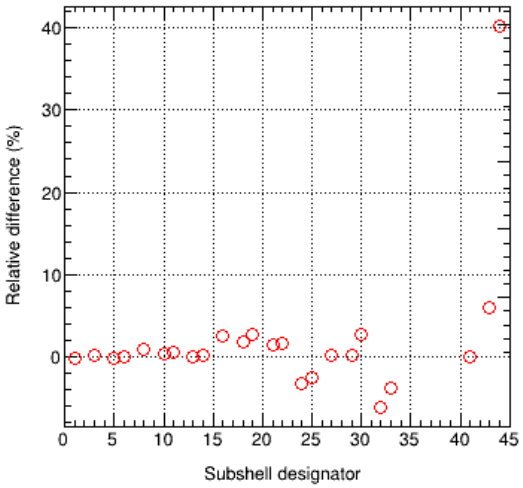
Relative difference (%)
Subshell designator

FigB5

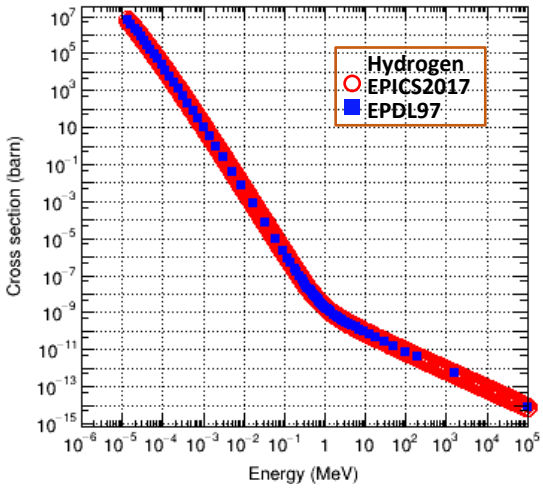
Hydrogen
EPICS2017
EPDL97
Cross section (barn)
Energy (MeV)

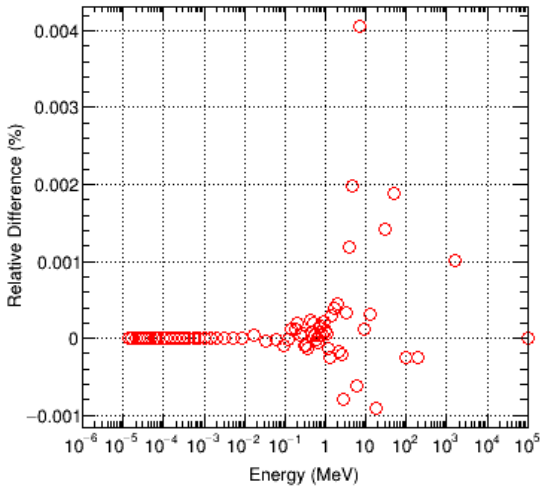
Relative Difference (%)
Energy (MeV)

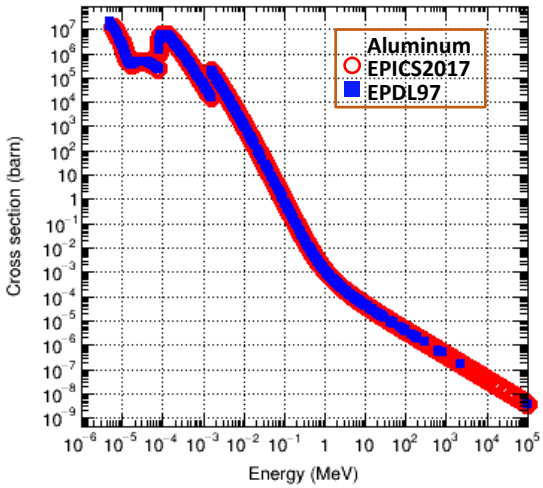
Aluminum
EPICS2017
EPDL97
Cross section (barn)
Energy (MeV)

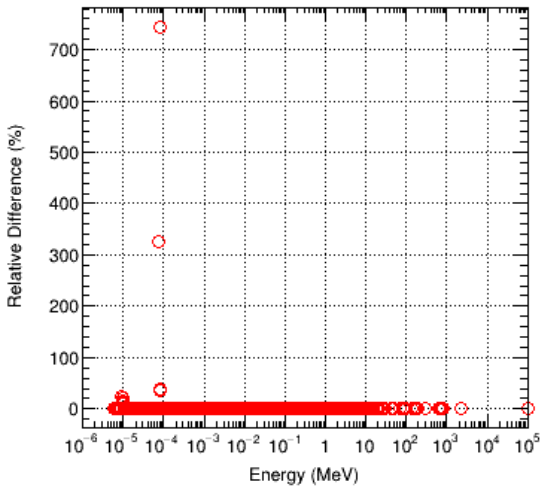
Relative Difference (%)
Energy (MeV)

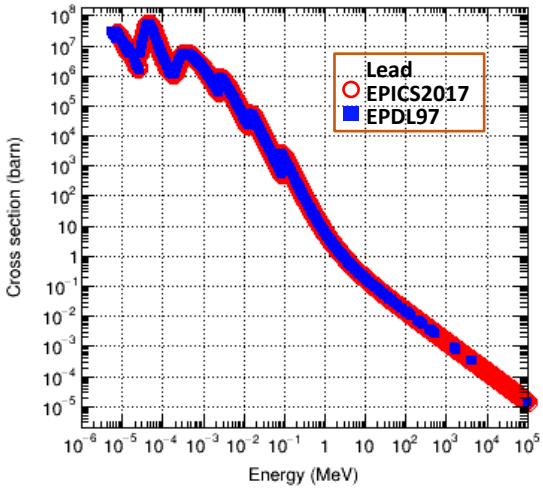
Lead
EPICS2017
EPDL97
Cross section (barn)
Energy (MeV)

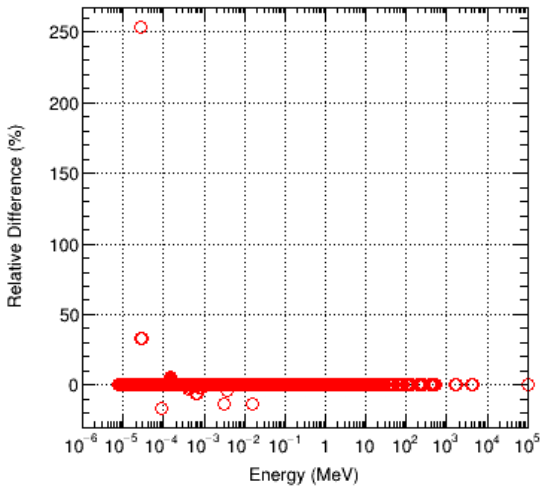
Relative Difference (%)
Energy (MeV)

FigB6

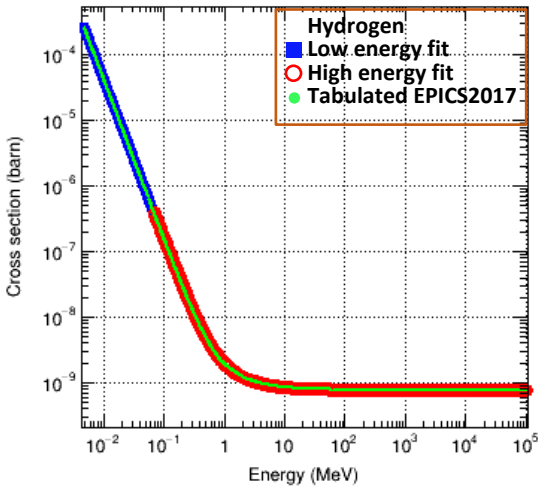
Hydrogen
Low energy fit
High energy fit
Tabulated EPICS2017
Cross section (barn)
Energy (MeV)

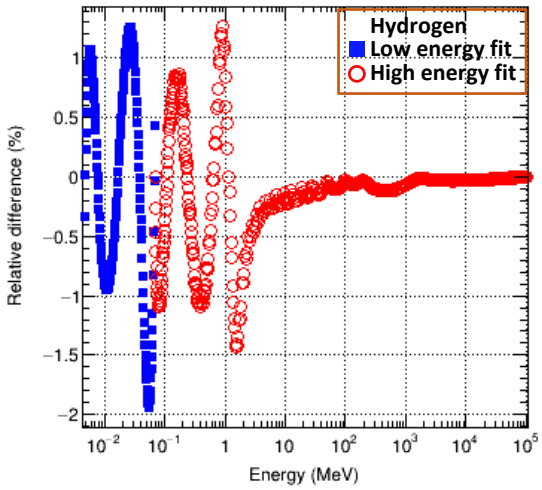
Hydrogen
Low energy fit
High energy fit
Relative difference (%)
Energy (MeV)

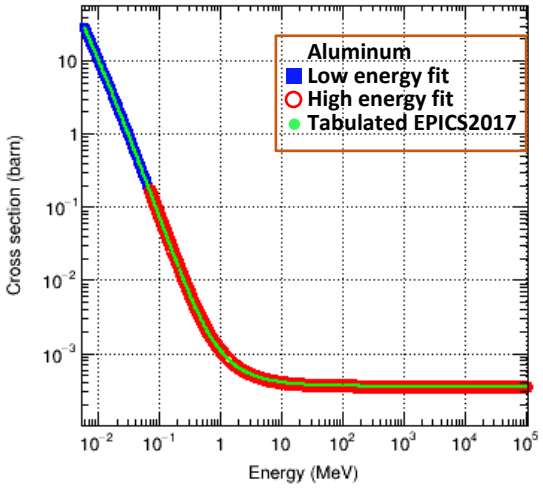
Aluminum
Low energy fit
High energy fit
Tabulated EPICS2017
Cross section (barn)
Energy (MeV)

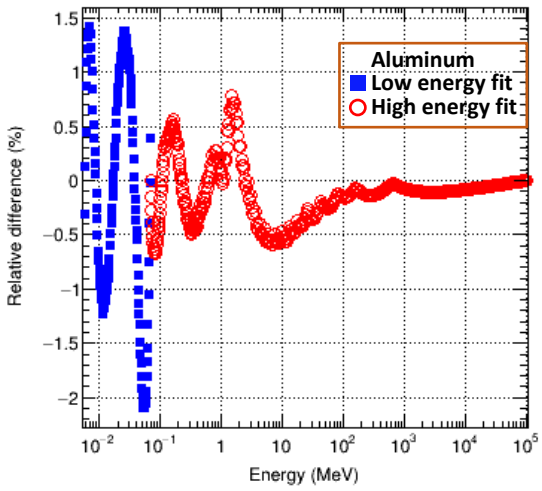
Aluminum
Low energy fit
High energy fit
Relative difference (%)
Energy (MeV)

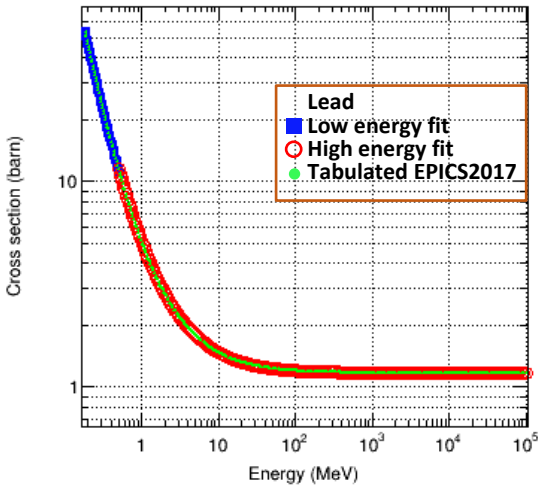
Lead
Low energy fit
High energy fit
Tabulated EPICS2017
Cross section (barn)
Energy (MeV)

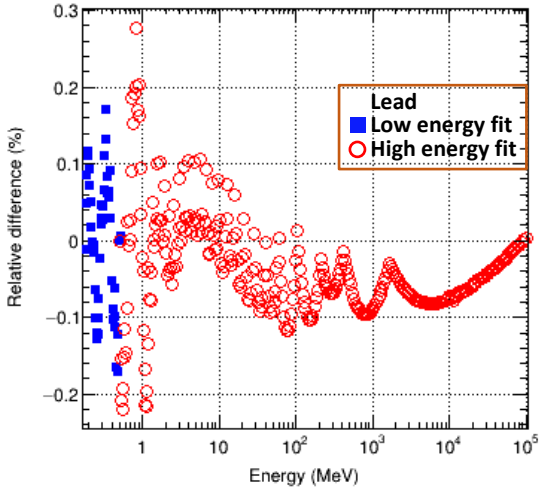
Lead
Low energy fit
High energy fit
Relative difference (%)
Energy (MeV)

FigB7

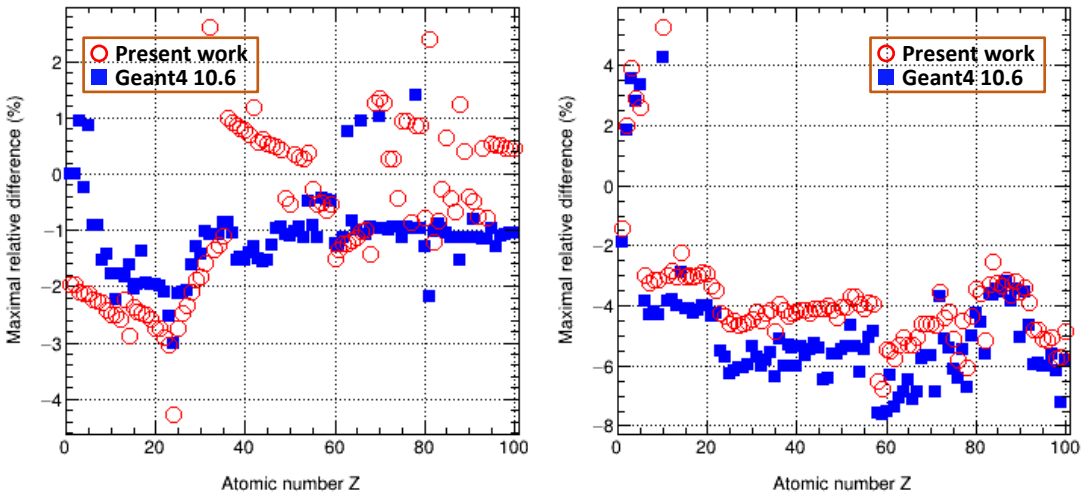
Present work
Geant4 10.6
Maximal relative difference (%)
Atomic number Z
Present work
Geant4 10.6
Maximal relative difference (%)
Atomic number Z

FigB8

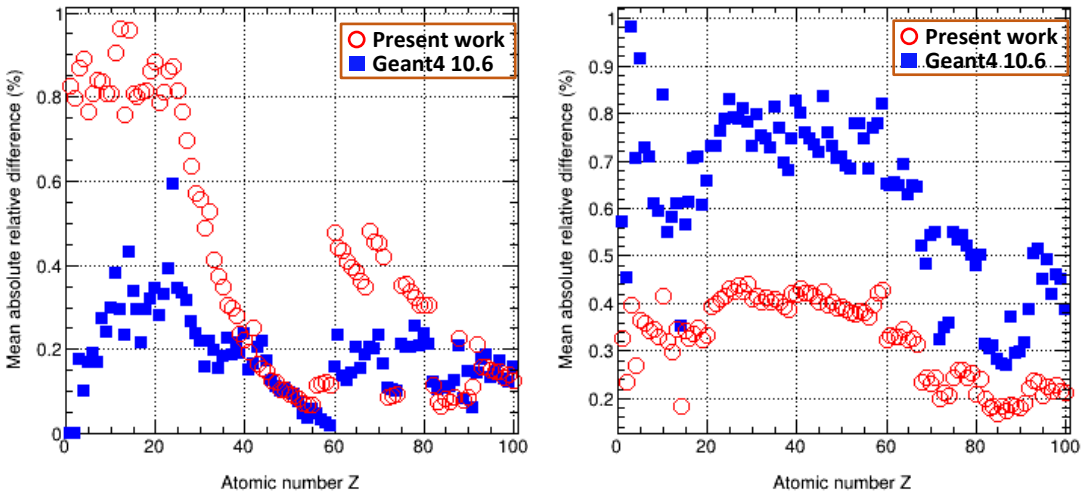
Present work
Geant4 10.6
Mean absolute relative difference (%)
Atomic number Z
Present work
Geant4 10.6
Mean absolute relative difference (%)
Atomic number Z

FigB9

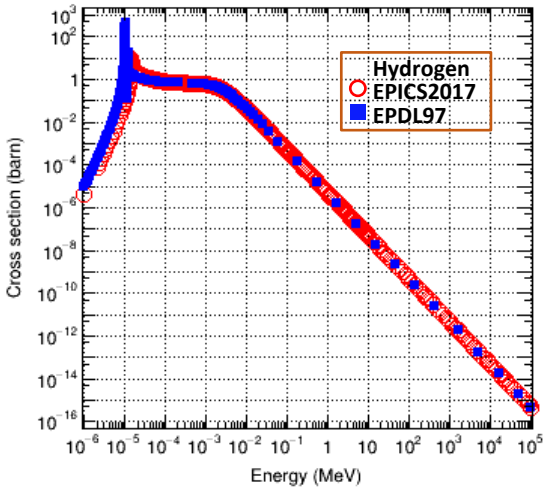
Hydrogen
EPICS2017
EPDL97
Cross section (barn)
Energy (MeV)

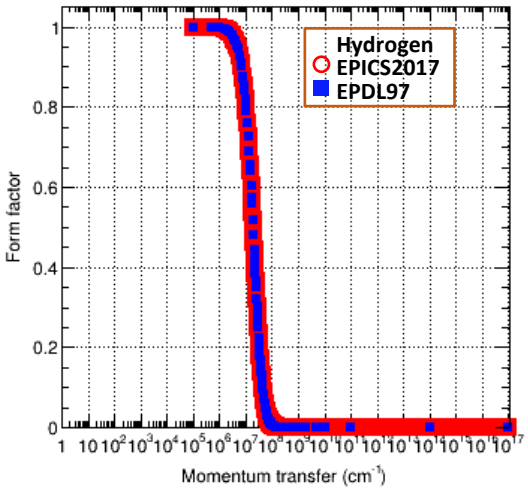
Hydrogen
EPICS2017
EPDL97
Form factor
Momentum transfer (cm^{-1})

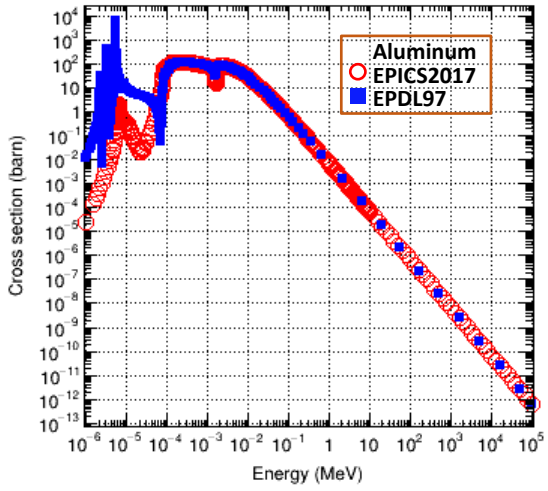
Aluminum
EPICS2017
EPDL97
Cross section (barn)
Energy (MeV)

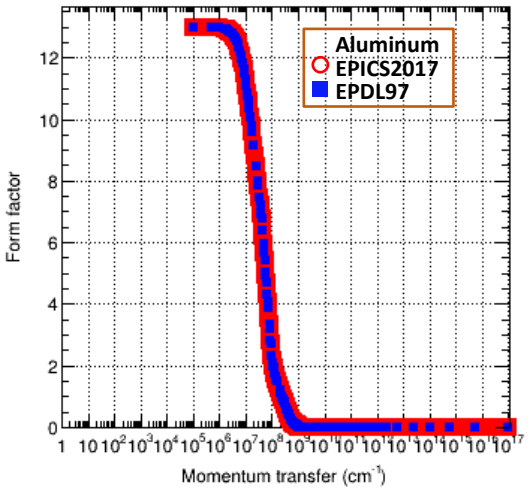
Aluminum
EPICS2017
EPDL97
Form factor
Momentum transfer (cm^{-1})

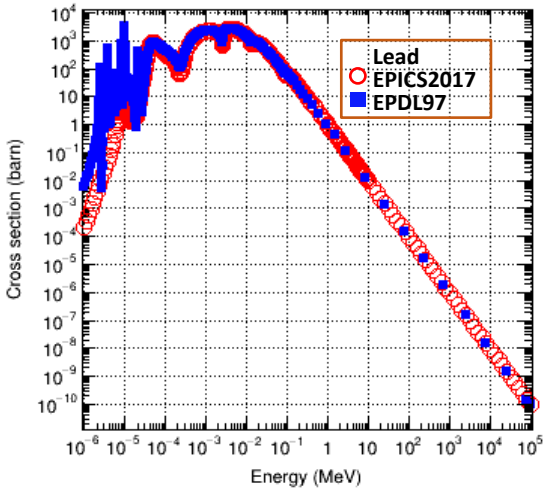
Lead
EPICS2017
EPDL97
Cross section (barn)
Energy (MeV)

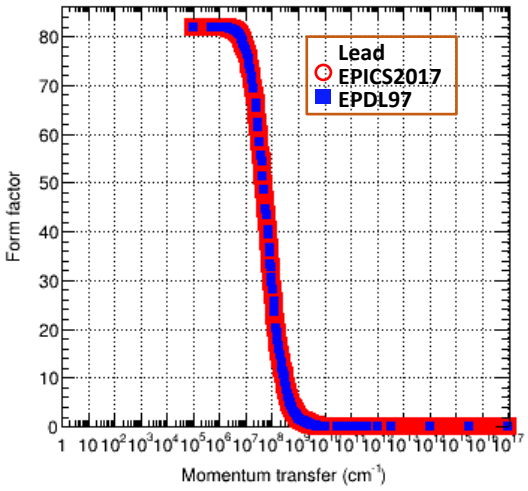
Lead
EPICS2017
EPDL97
Form factor
Momentum transfer (cm^{-1})

FigB10

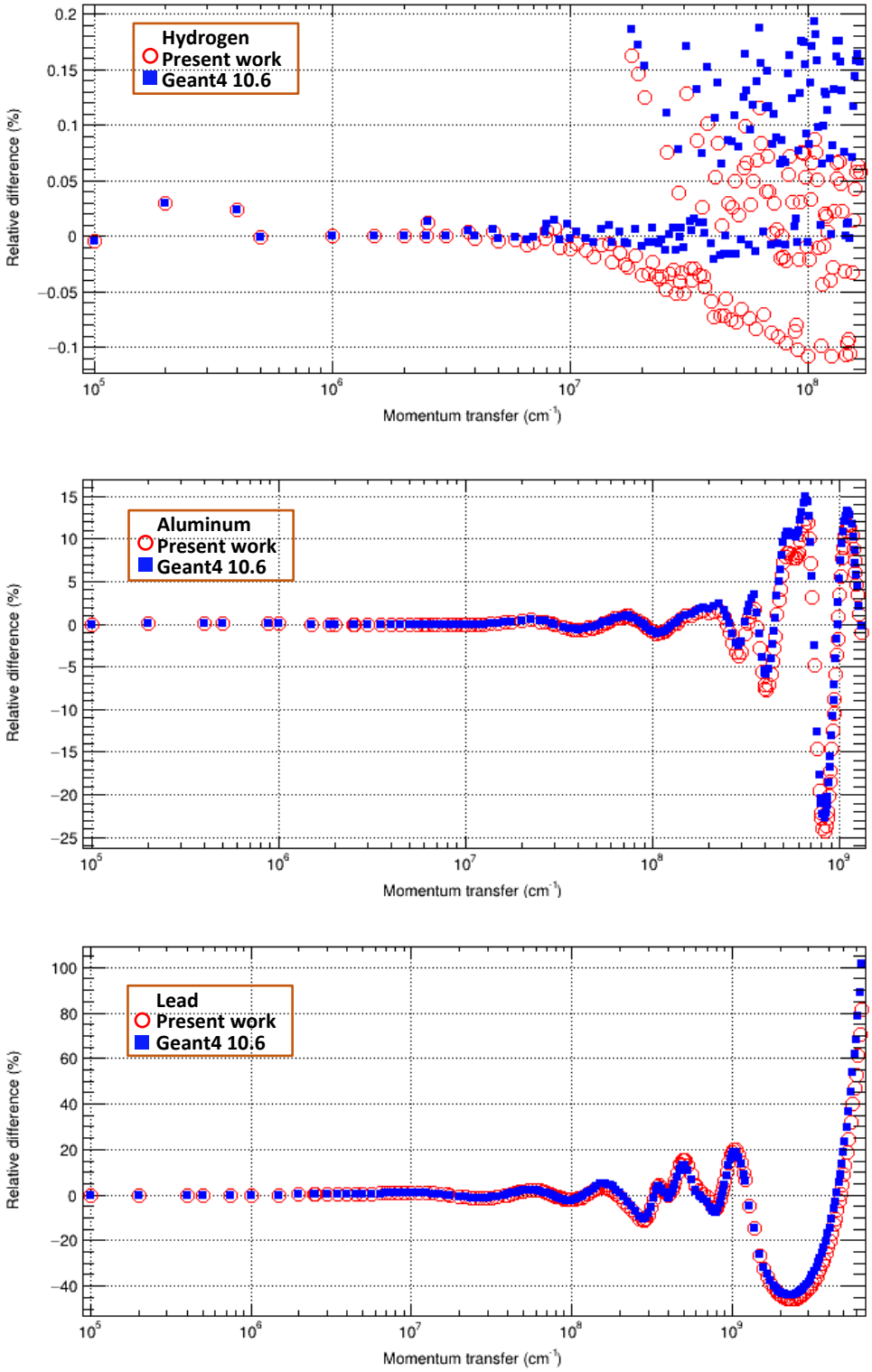
Hydrogen
Present work
Geant4 10.6
Relative difference (%)
Momentum transfer (cm^{-1})
Aluminum
Present work
Geant4 10.6
Relative difference (%)
Momentum transfer (cm^{-1})
Lead
Present work
Geant4 10.6
Relative difference (%)
Momentum transfer (cm^{-1})

FigB11

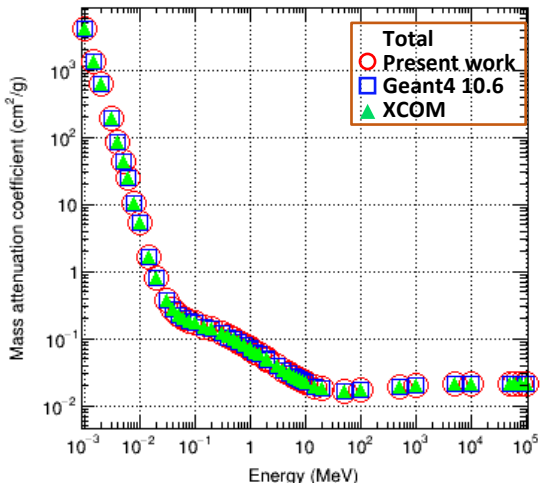
Total
Present work
Geant4 10.6
XCOM
Mass attenuation coefficient (cm²/g)
Energy (MeV)

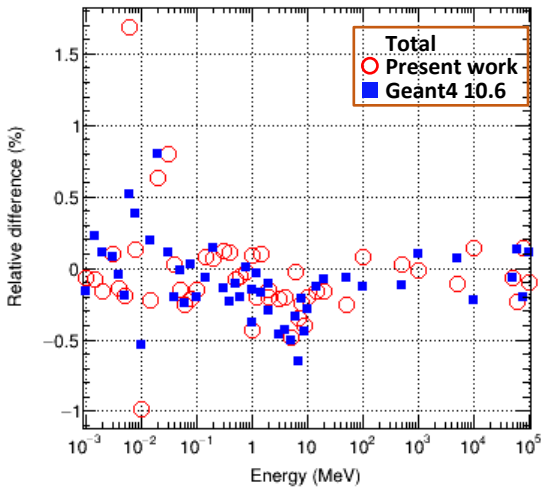
Total
Present work
Geant4 10.6
Relative difference (%)
Energy (MeV)

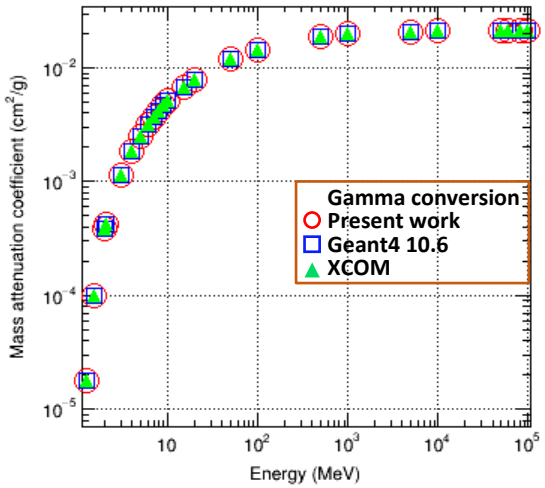
Gamma conversion
Present work
Geant4 10.6
XCOM
Mass attenuation coefficient (cm²/g)
Energy (MeV)

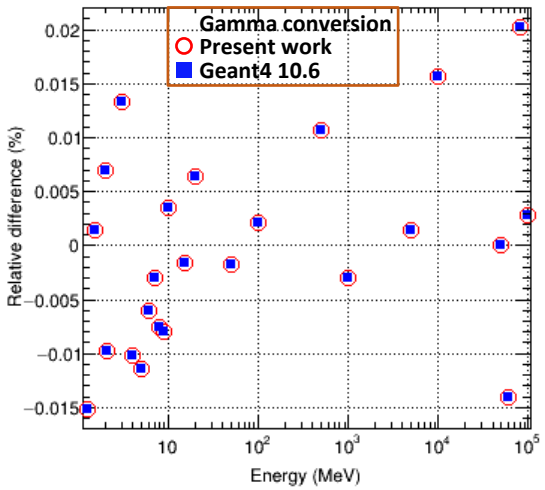
Gamma conversion
Present work
Geant4 10.6
Relative difference (%)
Energy (MeV)

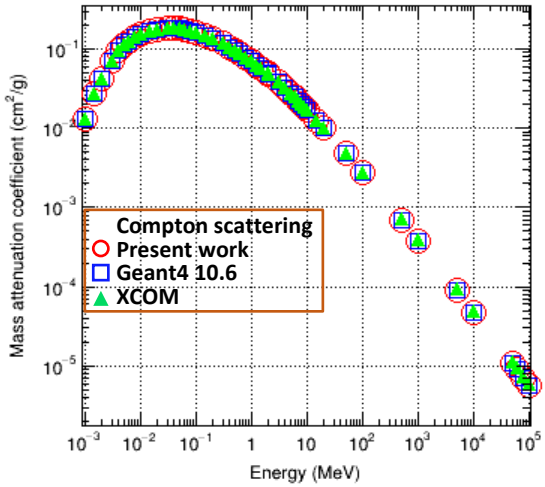
Compton scattering
Present work
Geant4 10.6
XCOM
Mass attenuation coefficient (cm²/g)
Energy (MeV)

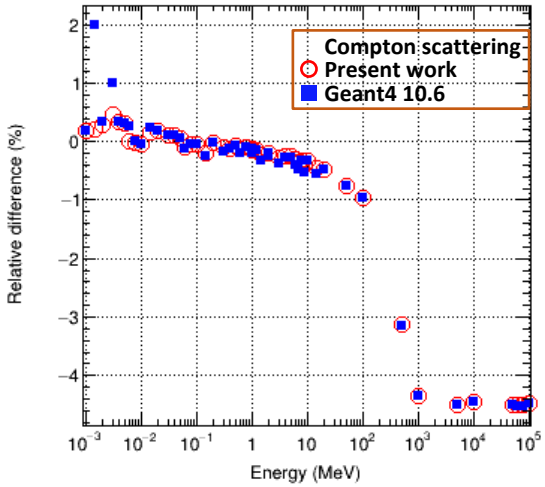
Compton scattering
Present work
Geant4 10.6
Relative difference (%)
Energy (MeV)

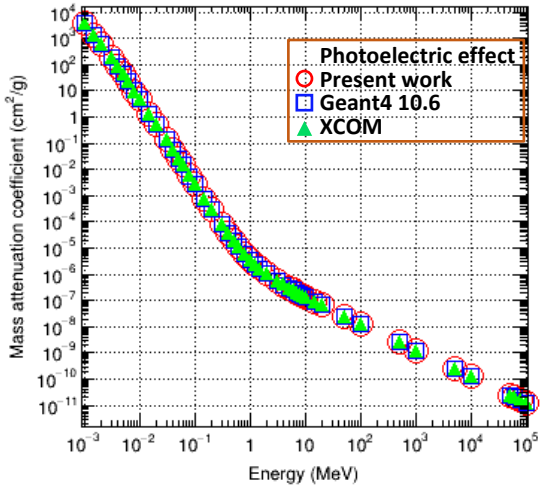
Photoelectric effect
Present work
Geant4 10.6
XCOM
Mass attenuation coefficient (cm²/g)
Energy (MeV)

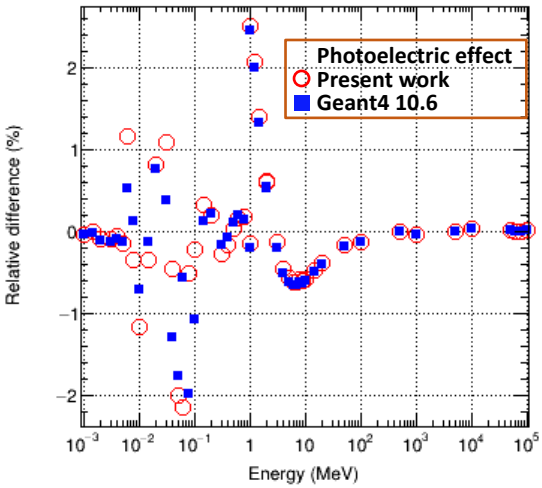
Photoelectric effect
Present work
Geant4 10.6
Relative difference (%)
Energy (MeV)

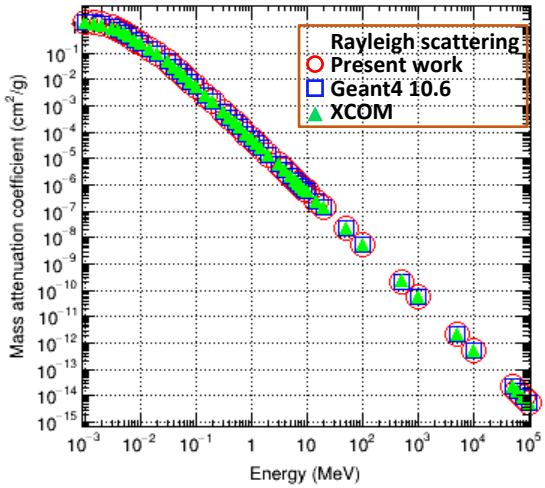
Rayleigh scattering
Present work
Geant4 10.6
XCOM
Mass attenuation coefficient (cm²/g)
Energy (MeV)

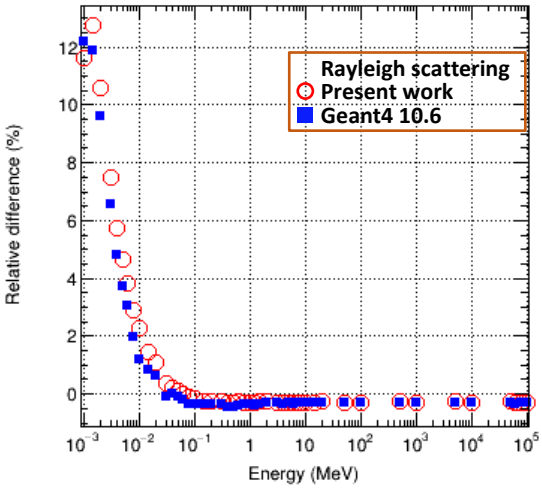
Rayleigh scattering
Present work
Geant4 10.6
Relative difference (%)
Energy (MeV)

FigB12

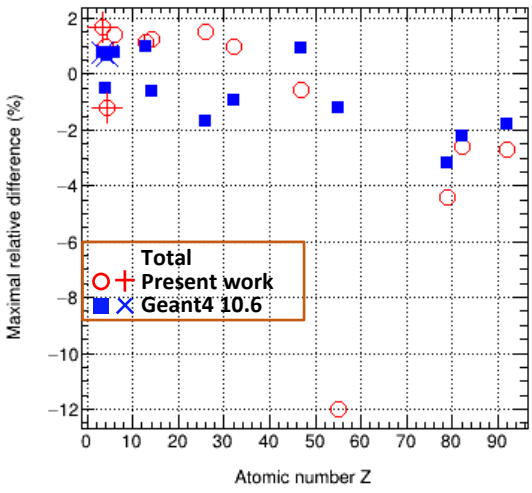
Total
Present work
Geant4 10.6
Maximal relative difference (%)
Atomic number Z

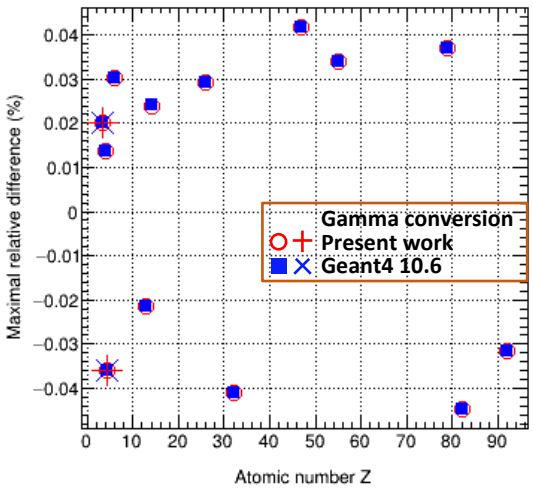
Gamma conversion
Present work
Geant4 10.6
Maximal relative difference (%)
Atomic number Z

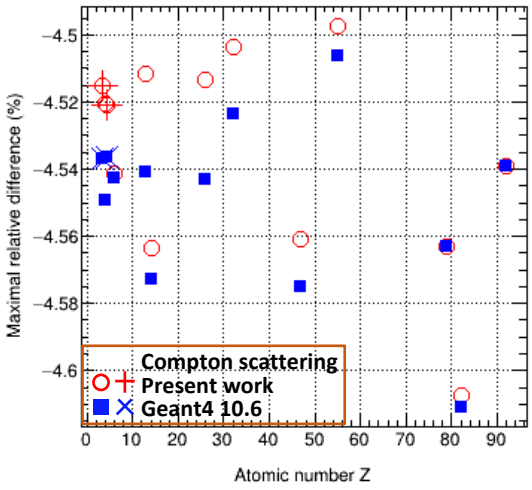
Compton scattering
Present work
Geant4 10.6
Maximal relative difference (%)
Atomic number Z

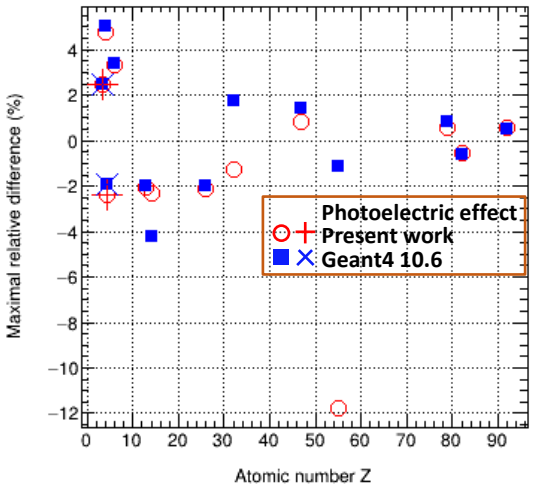
Photoelectric effect
Present work
Geant4 10.6
Maximal relative difference (%)
Atomic number Z

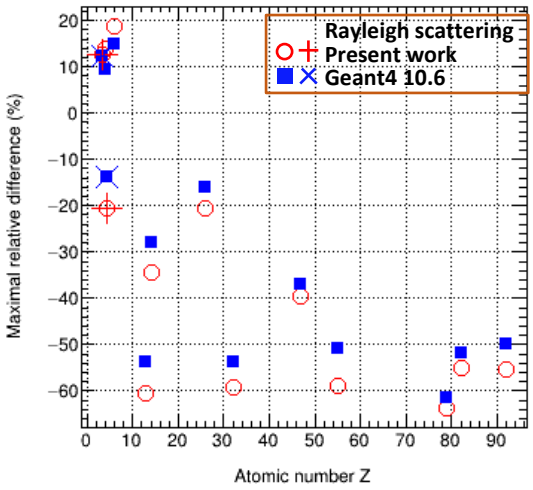
Rayleigh scattering
Present work
Geant4 10.6
Maximal relative difference (%)
Atomic number Z

FigB13

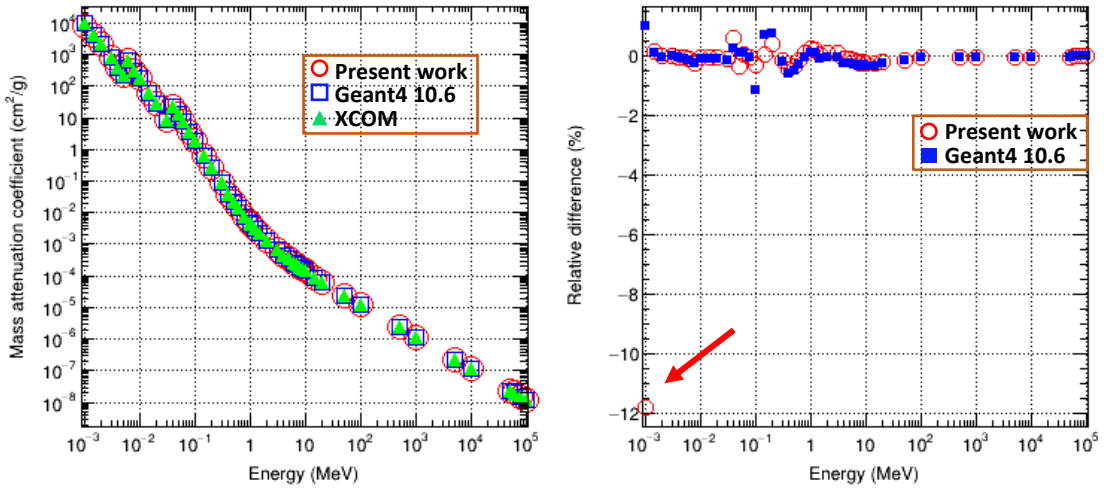
Present work
Geant4 10.6
XCOM
Mass attenuation coefficient (cm²/g)
Energy (MeV)
Present work
Geant4 10.6
Relative difference (%)
Energy (MeV)